# Nuclear Modification of Quarkonium Production in $p$+Pb Collisions at the LHC

**R. Vogt**

**Nuclear and Chemical Sciences Division,**
**Lawrence Livermore National Laboratory, Livermore, CA 94551, USA**

**Physics Department, University of California, Davis, CA 95616, USA**

# $J/\psi$ and $\Upsilon$ Production in $\sqrt{s_{NN}} = 5$ TeV $p$+Pb Collisions

- **Quarkonium production in $pp$ collisions**
- **Calculations of $R_{p\mathrm{Pb}}(p_T)$ at forward, backward, and midrapidity, $R_{p\mathrm{Pb}}(y)$, and forward/backward ratios $R_{FB}(p_T)$ and $R_{FB}(y)$**
  - **Dependence on proton PDF**
  - **EPS09 with nPDF uncertainties**
  - **LO vs NLO, EPS09 and nDS(g)**
  - **Central EPS09 compared to nDS(g), FGS-H, FGS-L and EKS98**
  - **Mass and scale uncertainties, EPS09 central set**
- **Factorization of cold matter effects: $R_{\mathrm{PbPb}}$ vs $R_{p\mathrm{Pb}} \times R_{\mathrm{Pb}p}$**

# Charmonium Family

## Extracting direct production

- **Subtract non-prompt decays ($b$ quark sources)**
- **Remaining $\psi'$ production is prompt**
- **Subtract $\psi'$ contributions to inclusive $J/\psi$**
- **Determine prompt $\chi_{cJ}$ production from $\chi_{cJ} \to J/\psi\gamma$ decays**
- **Subtract $\chi_{cJ}$ contributions to inclusive $J/\psi$**
- **Remaining $J/\psi$ production is prompt**

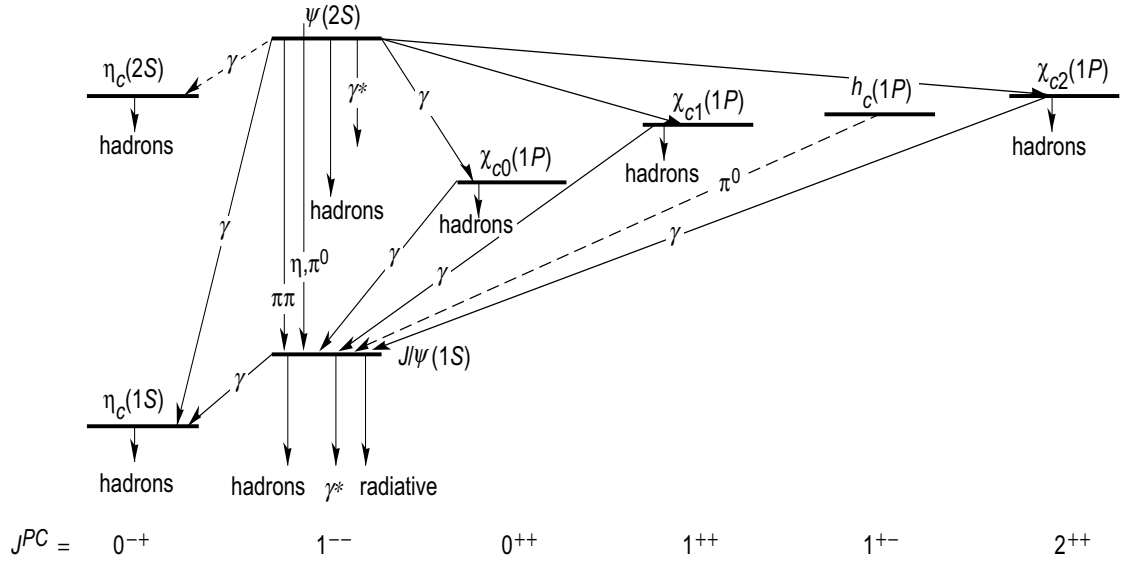


Figure 1: Spectrum of the charmonium family with important decay transitions between states highlighted.

# Bottomonium Family

**Extracting direct $\Upsilon(1S)$ production more complicated: many $b\overline{b}$ states below the $B\overline{B}$ threshold**

- **All $\Upsilon''$ production is prompt**
- **Direct $\Upsilon'$ production requires subtraction of $\Upsilon'' \to \Upsilon'$ and $\chi_b(2P) \to \Upsilon'$ from inclusive $\Upsilon'$**
- **Direct $\Upsilon$ production requires subtraction of $\Upsilon'' \to \Upsilon$, $\chi_b(2P) \to \Upsilon$, inclusive $\Upsilon' \to \Upsilon$ and inclusive $\chi_b(1P) \to \Upsilon$**

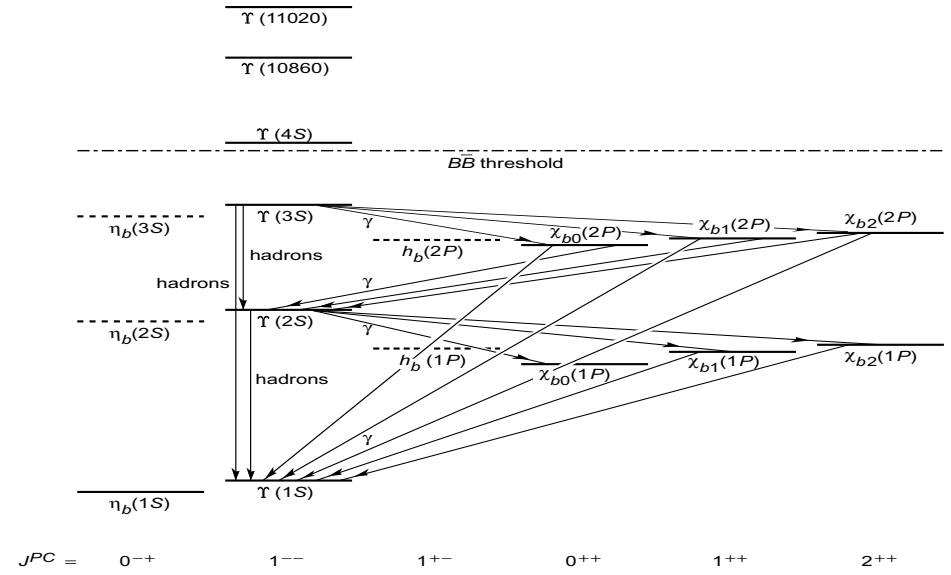


Figure 2: Spectrum of the bottomonium family with important decay transitions between states highlighted.

# $J/\psi$ Calculation in NLO CEM Based on Fitting $\sigma_{c\bar{c}}$

**Caveat: full NNLO cross section unknown, could still be large corrections**

**Employ $m = 1.27$ GeV, lattice value at $m(3\,\mathrm{GeV})$ and use subset of $c\bar{c}$ total cross section data to fix $\mu_F/m$ $(2.1^{+2.55}_{-0.85})$ and $\mu_R/m$ $(1.6^{+0.11}_{-0.12})$ with CT10 PDFs**

**Result with $\Delta\chi^2 = 1$ gives uncertainty on scale parameters; $\Delta\chi^2 = 2.3$ gives one standard deviation on total cross section**

**LHC $pp \to c\bar{c}$ at $\sqrt{s} = 7$ TeV not included but agrees well**

**The $c\bar{c}$ mass and scale parameters are used to calculate $J/\psi$ production**

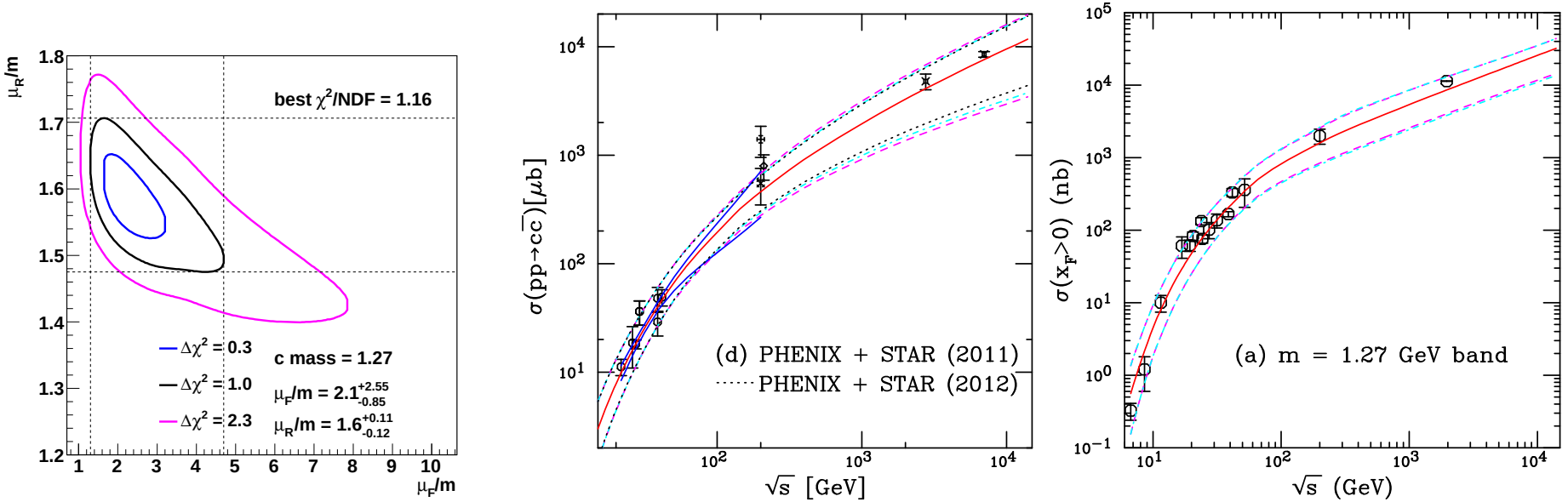


Figure 3: (Left) The $\chi^2$/dof contours for fits including the STAR 2011 cross section but excluding the STAR 2004 cross section. The best fit values are given for the furthest extent of the $\Delta\chi^2 = 1$ contours. (Center) The energy dependence of the charm total cross section compared to data. The best fit values are given for the furthest extent of the $\Delta\chi^2 = 1$ contours. The central value of the fit in each case is given by the solid red curve while the dashed magenta curves and dot-dashed cyan curves show the extent of the corresponding uncertainty bands. The dashed curves outline the most extreme limits of the band. In addition, the dotted black curves show the uncertainty bands obtained with the 2012 STAR results while the solid blue curves in the range $19.4 \le \sqrt{s} \le 200$ GeV represent the uncertainty obtained from the extent of the $\Delta\chi^2 = 2.3$ contour. (Right) The uncertainty band on the forward $J/\psi$ cross section. The dashed magenta curves and dot-dashed cyan curves show the extent of the corresponding uncertainty bands. The dashed curves outline the most extreme limits of the band. (RV, R Nelson and A D Frawley, Phys. Rev. C **87** (2013) 014908.)

# Results on LHC Charm Distributions

**Excellent agreement with $\sqrt{s} = 7$ TeV ALICE $pp$ data on muons in the forward region $(2.5 < y < 4)$**

**Leptons from semi-leptonic heavy flavor decays include contributions from $D \to \mu X$, $B \to \mu X$, $B \to D \to \mu X$, all with $\sim 10\%$ decay branching ratios**

**Fit results gives narrower uncertainty without reducing agreement with data than fiducial results based on $m = 1.5$ GeV**

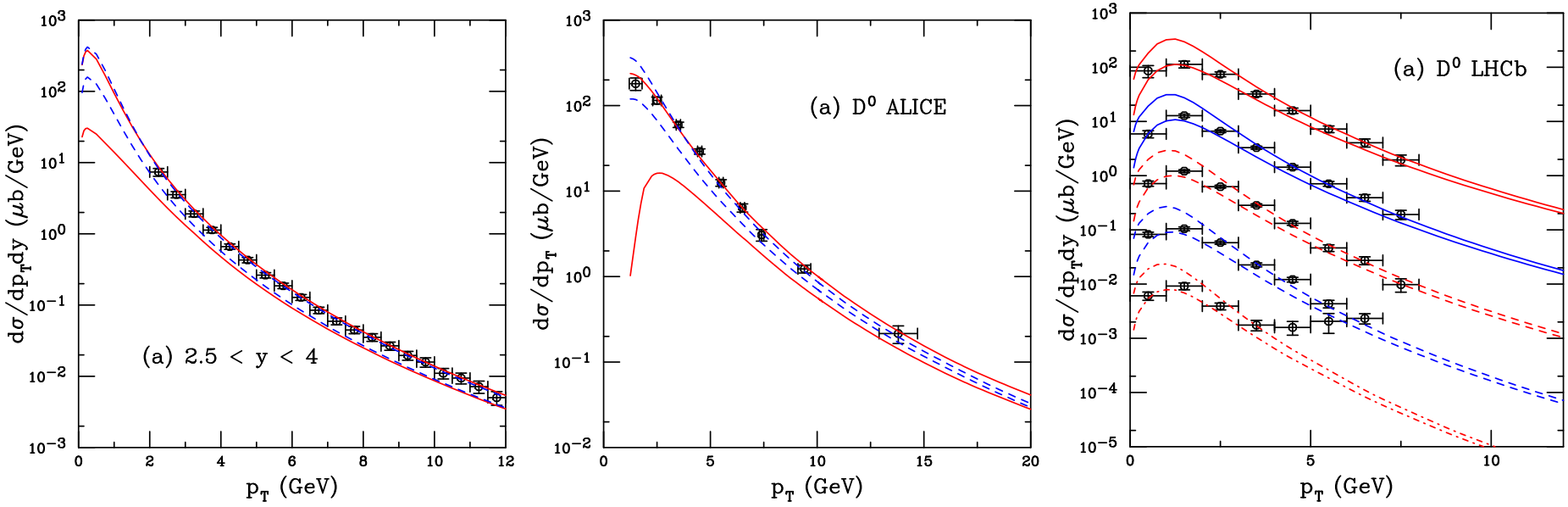


Figure 4: (Left) Comparison of the single lepton $p_T$ distributions in the rapidity interval $2.5 < y < 4$ at $\sqrt{s} = 7$ TeV calculated with the FONLL set for charm (solid red) and the fitted set with $m = 1.27$ GeV (dashed black). (Center) Our calculations are compared with the reconstructed ALICE $D^0$ data in $|y| \leq 0.5$. The FONLL uncertainty bands with the fiducial charm parameter set are shown by the red solid curves while the blue dashed curves are calculated with the charm fit parameters. (Right) Our calculations are compared with the reconstructed LHCb $D^0$ data in the rapidity intervals: $2 < y < 2.5$ (solid red); $2.5 < y < 3$ (solid blue); $3 < y < 3.5$ (dashed red); $3.5 < y < 4$ (dashed blue); and $4 < y < 4.5$ (dot-dashed red). The rapidity intervals are separated by a factor of 10 to facilitate comparison. The lowest rapidity interval, $2 < y < 2.5$, is not scaled. (RV, R Nelson and A D Frawley, Phys. Rev. C **87** (2013) 014908.)

# Comparison to ALICE $J/\psi$ $pp$ Distributions

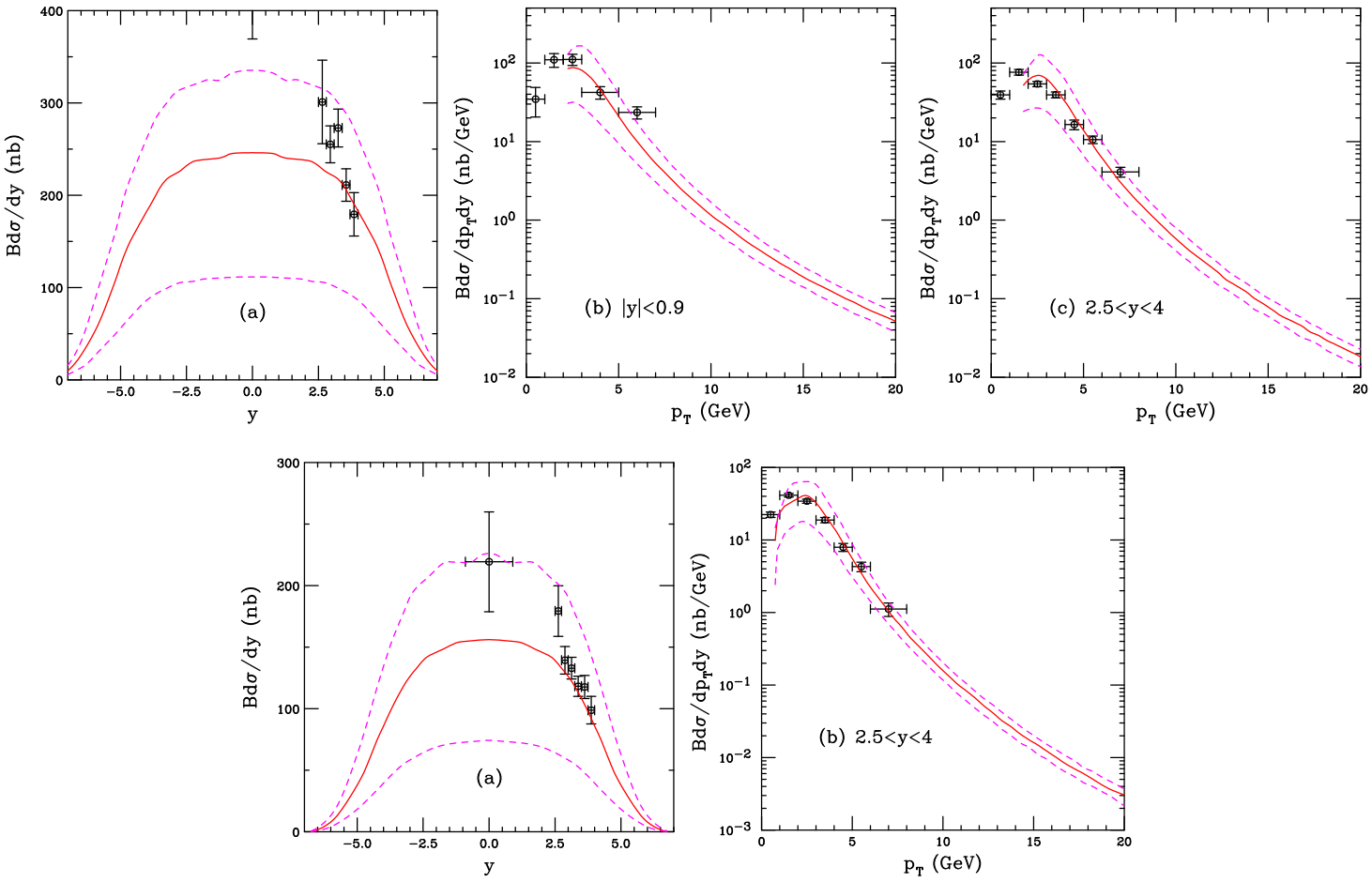


Figure 5: The $J/\psi$ rapidity distribution (a) and the midrapidity, $|y| < 0.9$ (b), and forward rapidity, $2.5 < y < 4$ (c) $p_T$ distributions at $\sqrt{s} = 7$ TeV (top) and 2.76 TeV (bottom) and their uncertainties. The results are compared to the ALICE rapidity distribution as well as the $p_T$ distributions. The solid red curve shows the central value while the dashed magenta curves outline the uncertainty band. A $\langle k_T^2 \rangle$ kick of 1.49 GeV$^2$ is applied to the $p_T$ distributions, as discussed in the text. (RV, R Nelson and A D Frawley, Phys. Rev. C **87** (2013) 014908.)

# $\Upsilon$ Calculation in NLO CEM Based on Fitting $\sigma_{b\bar{b}}$

**Caveat: full NNLO cross section unknown, could still be large corrections**

**Employ $m = 4.65$ GeV and use $b\bar{b}$ total cross section data to fix $\mu_F/m$ $(1.4^{+0.75}_{-0.47})$ and $\mu_R/m$ $(1.1^{+0.26}_{-0.19})$ with CT10 PDFs**

**Result with $\Delta\chi^2 = 1$ gives uncertainty on scale parameters; $\Delta\chi^2 = 2.3$ gives one standard deviation on total cross section**

**LHC $pp \to b\bar{b}$ at $\sqrt{s} = 7$ TeV included in fits, not enough reliable data at fixed target to help constrain**

**The $b\bar{b}$ mass and scale parameters are used to calculate $\Upsilon$ production**

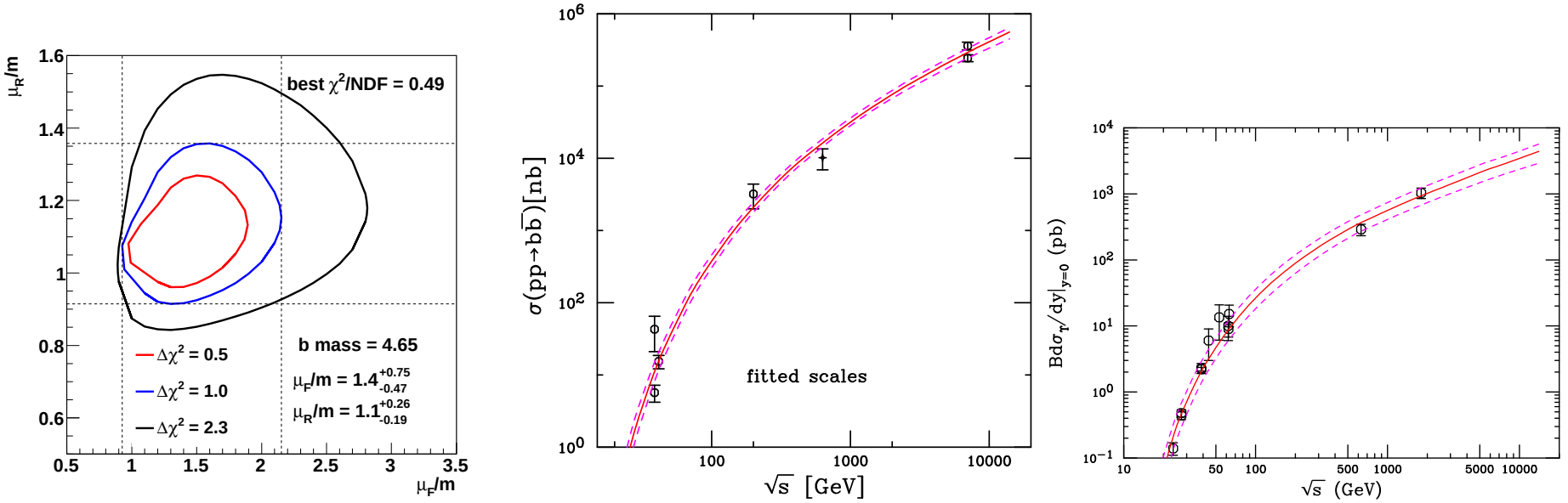


Figure 6: (Left) The $\chi^2$/dof contours for fits. The best fit values are given for the furthest extent of the $\Delta\chi^2 = 1$ contours. (Center) The energy dependence of the bottom total cross section compared to data. The best fit values are given for the furthest extent of the $\Delta\chi^2 = 1$ contours. The central value of the fit in each case is given by the solid red curve while the dashed magenta curves show the corresponding uncertainty bands. (Right) The uncertainty band on the $\Upsilon$ cross section at $y = 0$. The dashed magenta curves show the extent of the corresponding uncertainty bands. (RV, R Nelson and A D Frawley, in progress)

# Results for Bottom Distributions at the LHC

**Good agreement with ALICE inclusive single muon distributions (left) with calculations based on charm and bottom fits**

**Both $B$ hadron (center) and muons from $b$ decays (right) show agreement with the $p_T$ distributions**

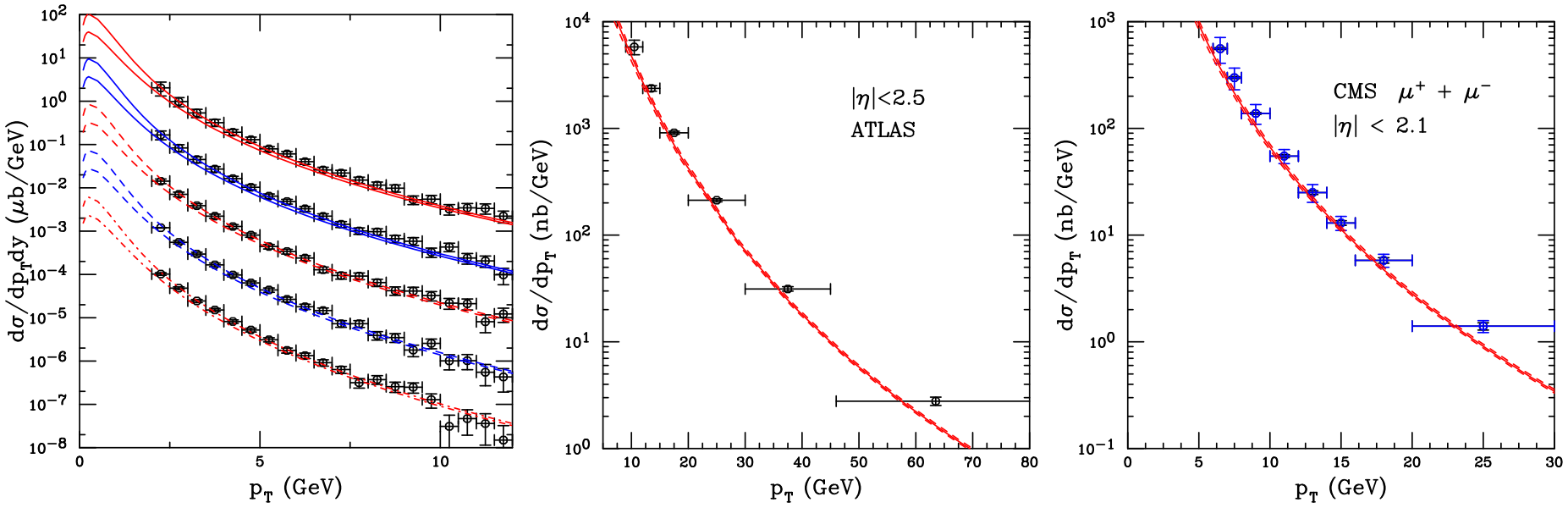


Figure 7: (Left) The ALICE inclusive single muon data from heavy flavor decays at $\sqrt{s} = 7$ TeV divided into rapidity bins, from top to bottom: $2.5 < y < 2.8$ (solid red); $2.8 < y < 3.1$ (solid blue); $3.1 < y < 3.4$ (dashed red); $3.4 < y < 3.7$ (dashed blue); and $3.7 < y < 4$ (dot-dashed red). The top curves are shown at their calculated value, the others are scaled down by successive factors of 10 to separate them. (Center) The $B$ hadron $p_T$ distribution measured by ATLAS. (Right) The muon $p_T$ distribution from $b$ decays measured by CMS. The calculations are with the central fit set and the one standard deviation in mass and scale values. (RV, R Nelson and A D Frawley, in progress)

# Comparison to $p\overline{p}$ and $pp$ $\Upsilon$ Data

**Need a larger broadening for the higher mass $b$ quarks**

**Good agreement with Tevatron Run II data, both in the full rapidity range and separated into different rapidity regions**

**Agreement with CMS $\Upsilon$ data for $p_T < 30$ GeV, very high $p_T$ hard to reproduce, requires high $p_T$ resummation for logs of large $p_T/m$**

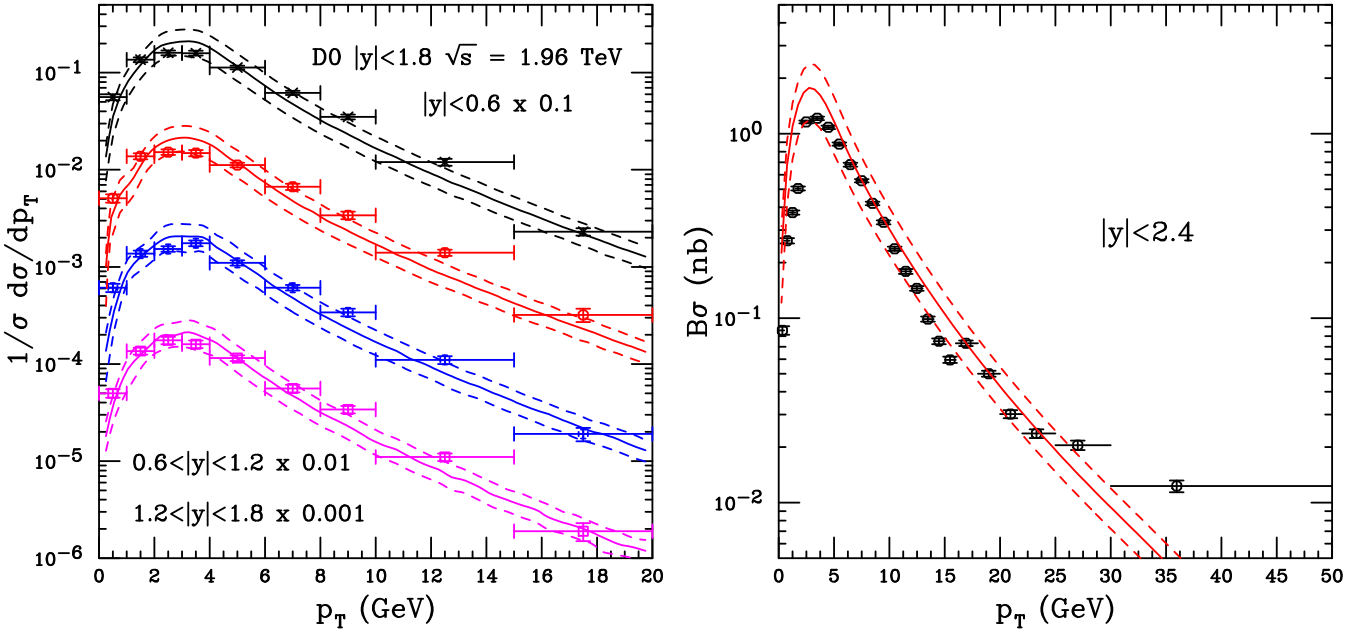


Figure 8: (Left) $\Upsilon(1S)$ $p_T$ distribution in the full measured rapidity range, $|y| < 1.8$ (black), and different rapidity bins: $|y| < 0.8$ (red); $0.8 < |y| < 1.2$ (blue); and $1.2 < |y| < 1.8$ (magenta). The data are from the D0 collaboration with $\sqrt{s} = 1.96$ TeV in $\overline{p}p$ collisions at the Tevatron. (Right) Calculation of the $\Upsilon(1S)$ $p_T$ distribution in $pp$ collisions at $\sqrt{s} = 7$ TeV. The data are from the CMS collaboration and are from the rapidity range $|y| < 2.4$. (RV, R Nelson and A D Frawley, in progress)

# Cold Nuclear Matter Effects in Hadroproduction

**In heavy-ion collisions, one has to fold in cold matter effects, typically studied in $pA$ or d$A$ interactions from fixed-target energies to colliders**

**Important cold nuclear matter effects in hadroproduction include:**

- **Initial-state nuclear effects on the parton densities (nPDFs)**
- **Initial- (or final-) state energy loss**
- **$k_T$ broadening from multiple scattering**
- **Final-state absorption on nucleons**
- **Final-state break up by comovers (hadrons or partons)**
- **Intrinsic $Q\overline{Q}$ pairs**

**After some very brief discussion of each, I will concentrate on nuclear parton densities (shadowing)**
**Open heavy flavor not affected by absorption or comover interactions**

# Cold Matter Effects Quantified by $A$ Dependence

**Open charm appears to be independent of $A$ ($N_{\rm bin}$) but quarkonium has a definite $A$ dependence**

**The $A$ dependence includes some or all of the aforementioned nuclear effects**

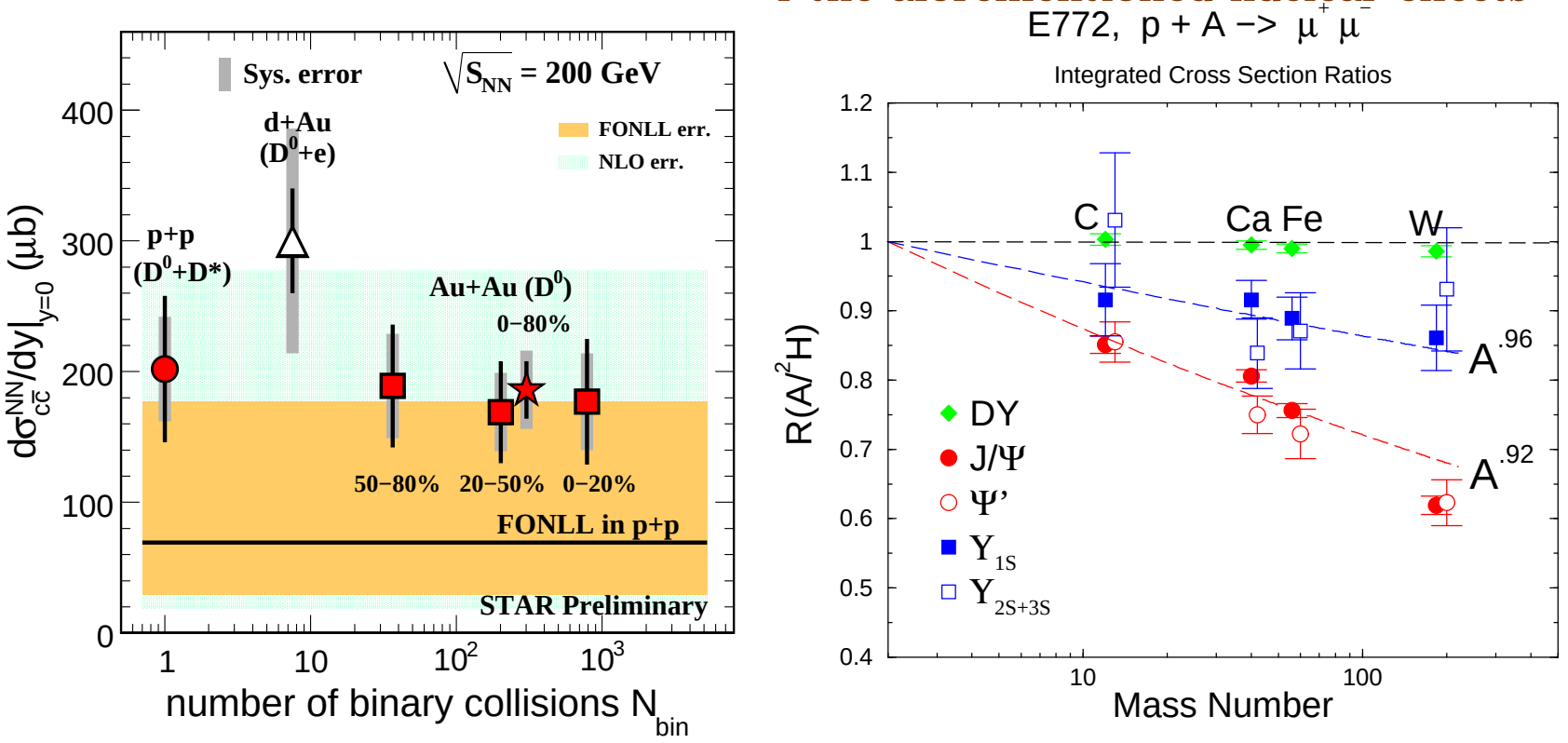


Figure 9: **(Left) The dependence of the open charm cross section on the number of binary collisions measured by the STAR Collaboration at central rapidity. (Right) The $A$ dependence of quarkonium and Drell-Yan production measured by E772.**

# E866 Measured Open Charm and $J/\psi$ vs $x_F$

**E866 also measured open charm $pA$ dependence using single muons with $p_T^\mu > 1$ GeV/$c$ (unpublished)**

**Different from $J/\psi$ for $y < 0.7$ but similar for higher $y$, suggests that dominant effects are in the initial state**

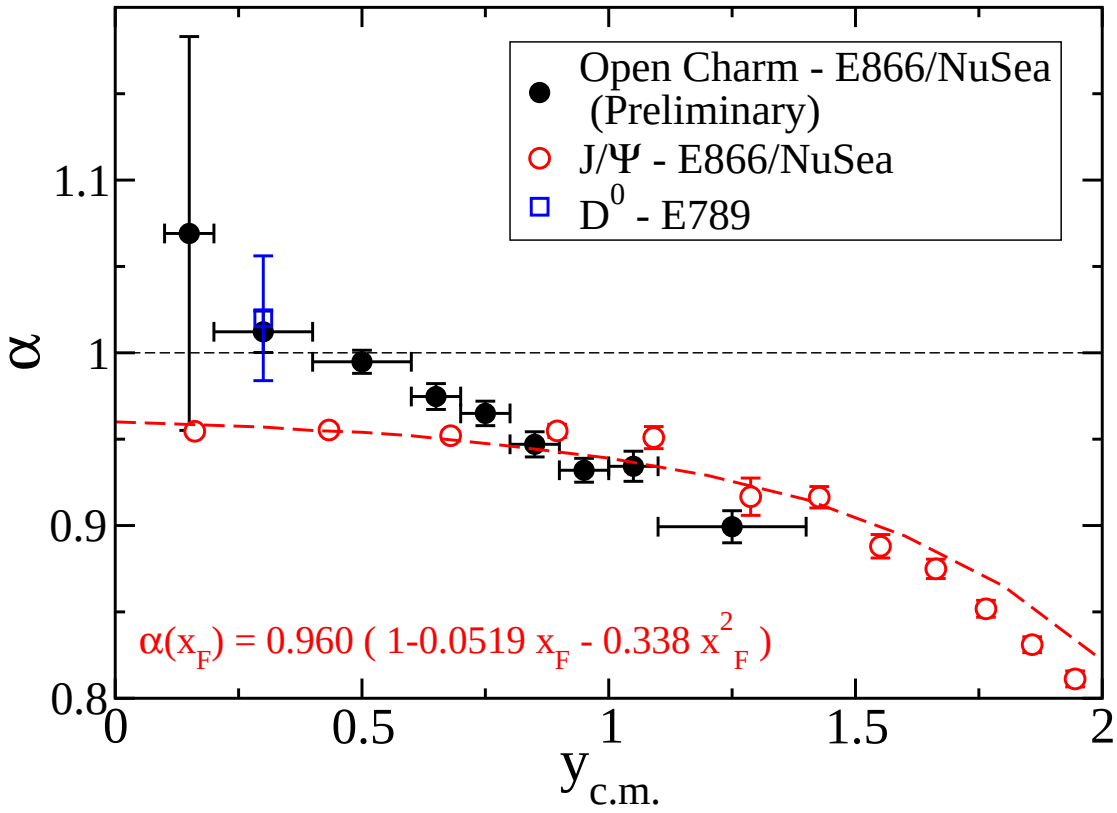


Figure 10: The $J/\psi$ and open charm $A$ dependence as a function of $x_F$ (Mike Leitch).

# Quick Tour of Cold Matter Effects

# Parton Densities Modified in Nuclei

## Nuclear deep-inelastic scattering measures quark modifications directly

## More uncertainty in nuclear gluon distribution, only indirectly constrained by $Q^2$ evolution of parton densities

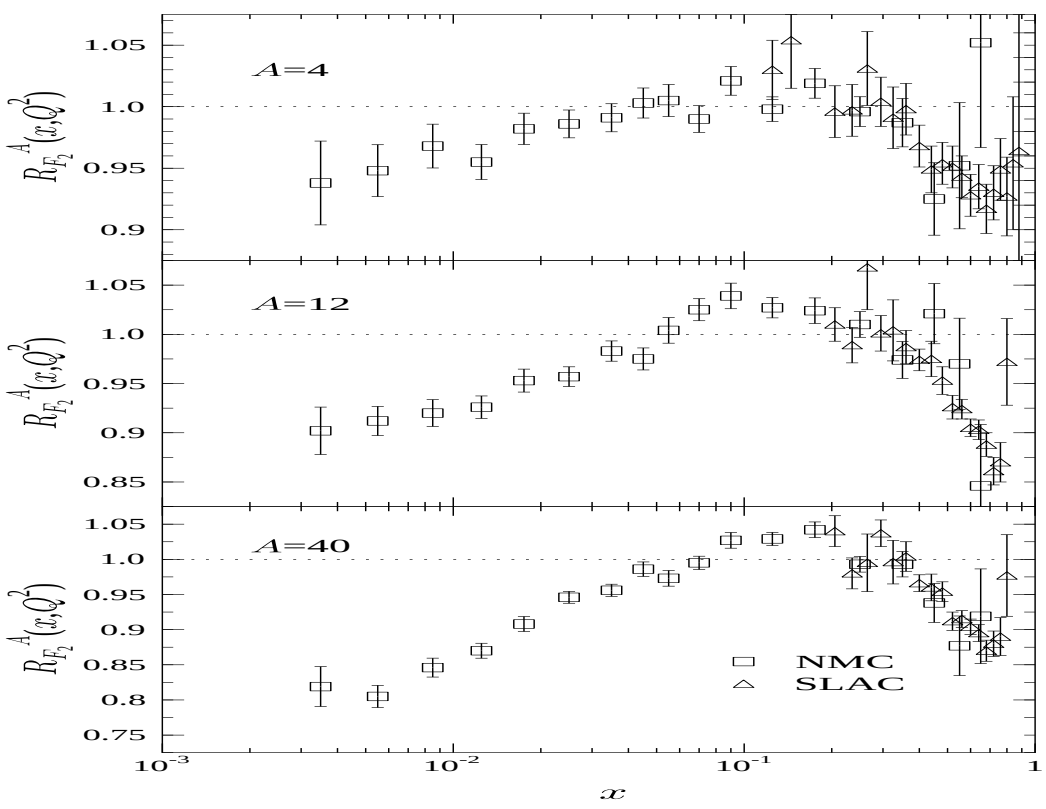


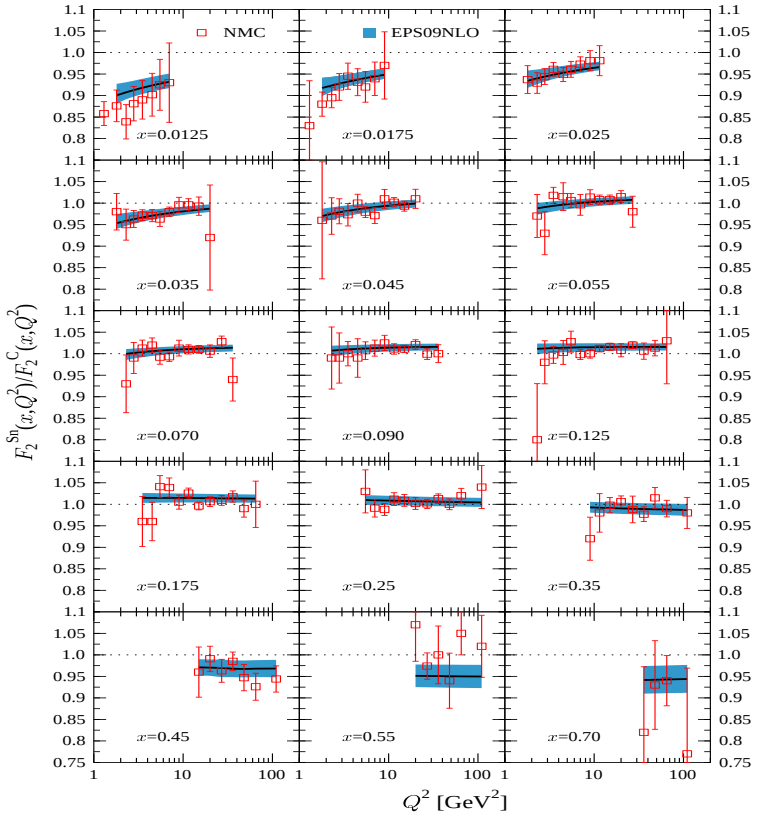


Figure 11: (Left) Ratios of charged parton densities in He, C, and Ca to D as a function of $x$. (Right) Evolution of gluon distributions in Sn relative to C targets with $Q^2$ for several fixed values of $x$. [From K.J. Eskola.]

# Why Shadowing Is Not All There Is

**Effective $\alpha$ dissimilar as a function of $x_2$, closer to scaling for $y_{\rm cm}$**

**At negative $x_F$, the HERA-B result suggests a negligible effective $J/\psi$ absorption cross section**

**Argument for more physics at forward $x_F$ than accounted for by nuclear shadowing**

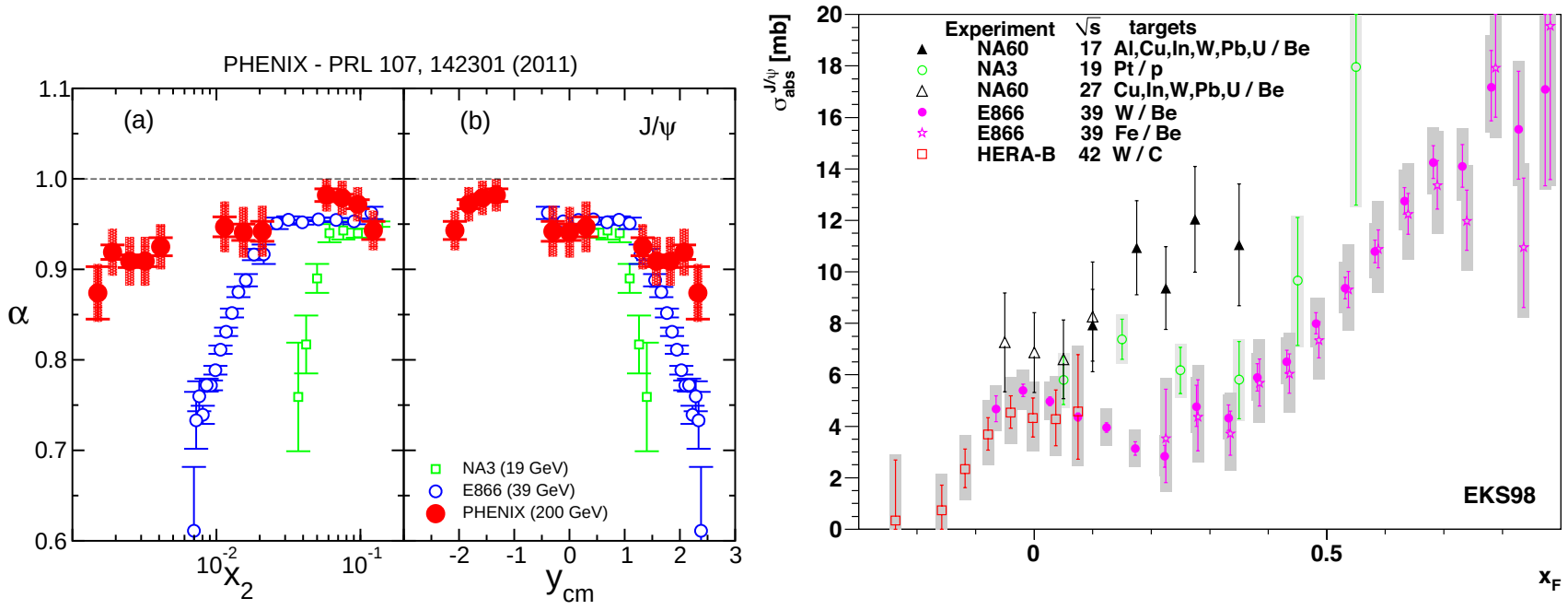


Figure 12: (Left) Comparison of effective $\alpha$ for NA3, E866 and PHENIX. (Mike Leitch) (Right) Comparison of effective $\sigma_{\rm abs}$ for $J/\psi$ (from QWG report, 2010).

# Parton Energy Loss Can Describe Trends

**Energy loss by multiple scattering in the initial (gluon) or final ($c\bar{c}$) state results in a backward shift in the longitudinal dependence**

**Same mechanism is responsible for $k_T$ broadening – what's lost to longitudinal kicks increases the average $p_T$ of the final state**

**Arleo *et al.* used a power law model of $pp$ collisions to implement final-state energy loss on $J/\psi$, results shown below agree for fixed target interactions, when shadowing is stronger there is a separation**

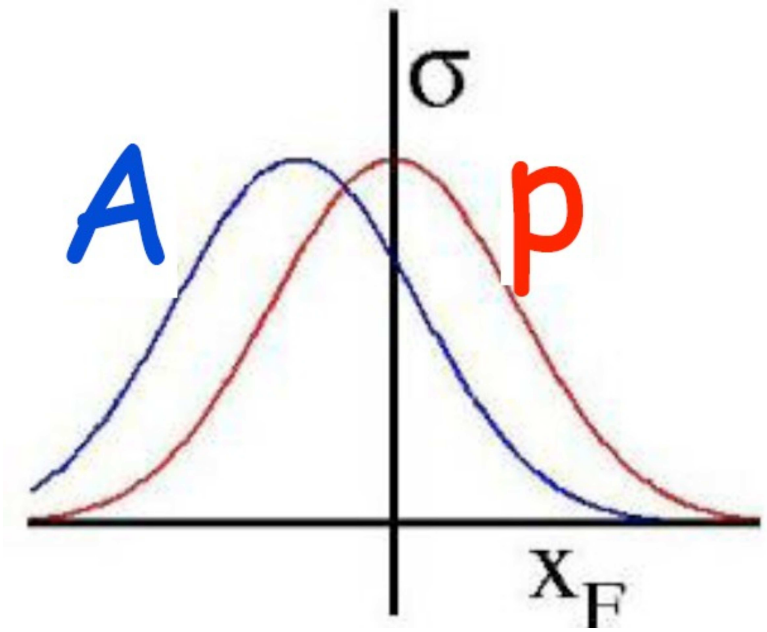


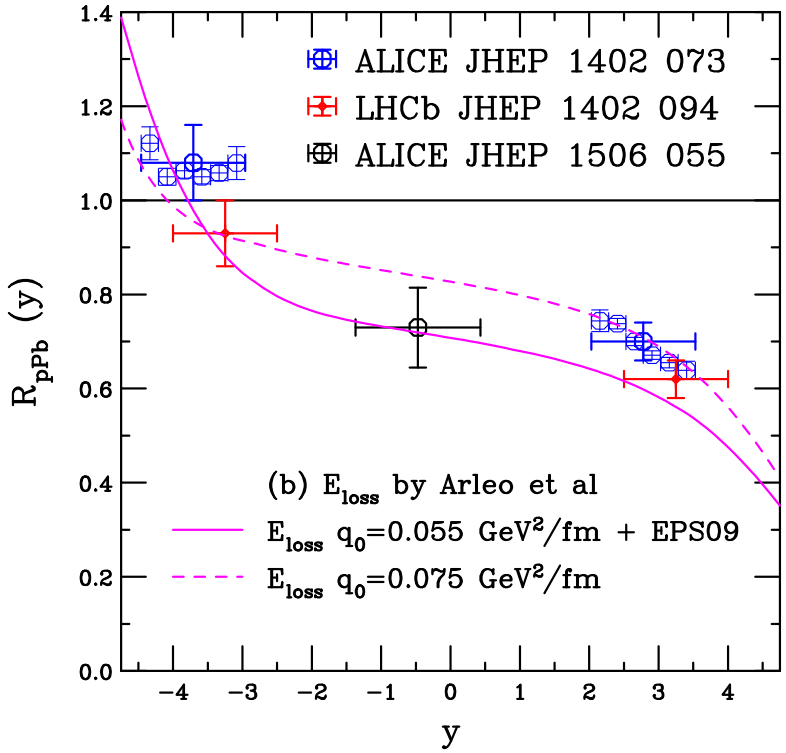


Figure 13: (Left) Shift in $x_F$ distribution caused by energy loss. (Mike Leitch) (Right) The LHC $J/\psi$ $R_{p\mathrm{Pb}}(y)$ data from ALICE and LHCb compared to energy loss model of Arleo *et al.*.

# Quarkonium Absorption

**Woods-Saxon nuclear density profiles typically used**

$$\begin{aligned}\sigma_{pA} &= \sigma_{pN}\int d^2b\int_{-\infty}^{\infty} dz\,\rho_A(b,z)S_A^{\rm abs}(b)\\ &= \sigma_{pN}\int d^2b\int_{-\infty}^{\infty} dz\,\rho_A(b,z)\exp\left\{-\int_z^{\infty} dz'\rho_A(b,z')\sigma_{\rm abs}(z'-z)\right\}\end{aligned}$$

**Note that if** $\rho_A=\rho_0$, $\alpha = 1-9\sigma_{\rm abs}/(16\pi r_0^2)$

**The value of** $\sigma_{\rm abs}$ **depends on the whether geometry is taken into account and how realistic that geometry is – hard sphere,** $A^\alpha$ **etc.**

**Effective** $\sigma_{\rm abs}$ **also depends on whether or not shadowing is taken into account**

**Feed down to** $J/\psi$ **from** $\chi_c$ **and** $\psi'$ **decays included**

$$\sigma_{pA} = \sigma_{pN}\int d^2b\,[0.6S^{\rm abs}_{A\,\psi,\,\rm dir}(b) + 0.3S^{\rm abs}_{A\,\chi_{cJ}}(b) + 0.1S^{\rm abs}_{A\,\psi'}(b)]$$

**Generally assume that each charmonium state interacts with a different, constant asymptotic absorption cross section but, with color singlets, the state grows until it reaches its asymptotic size, NRQCD approach would have different absorption cross sections with different dependence on rapidity,** $\sqrt{s}$ **for all states**

**The** $\chi_c$ $A$ **dependence remains unknown (PHENIX measured** $R_{\rm dAu}$ **similar to** $J/\psi$ **but with large uncertainties, no** $y$ **dependence**

# $A$ Dependence of $J/\psi$ and $\psi'$ Not Identical

**Fixed-target data sets (NA50 at SPS, E866 at FNAL) show clear difference at low $x_F$ (midrapidity)**

**At RHIC, $J/\psi$ production almost independent of centrality in d+Au collisions while $\psi'$ shows a very strong dependence. Comovers?**

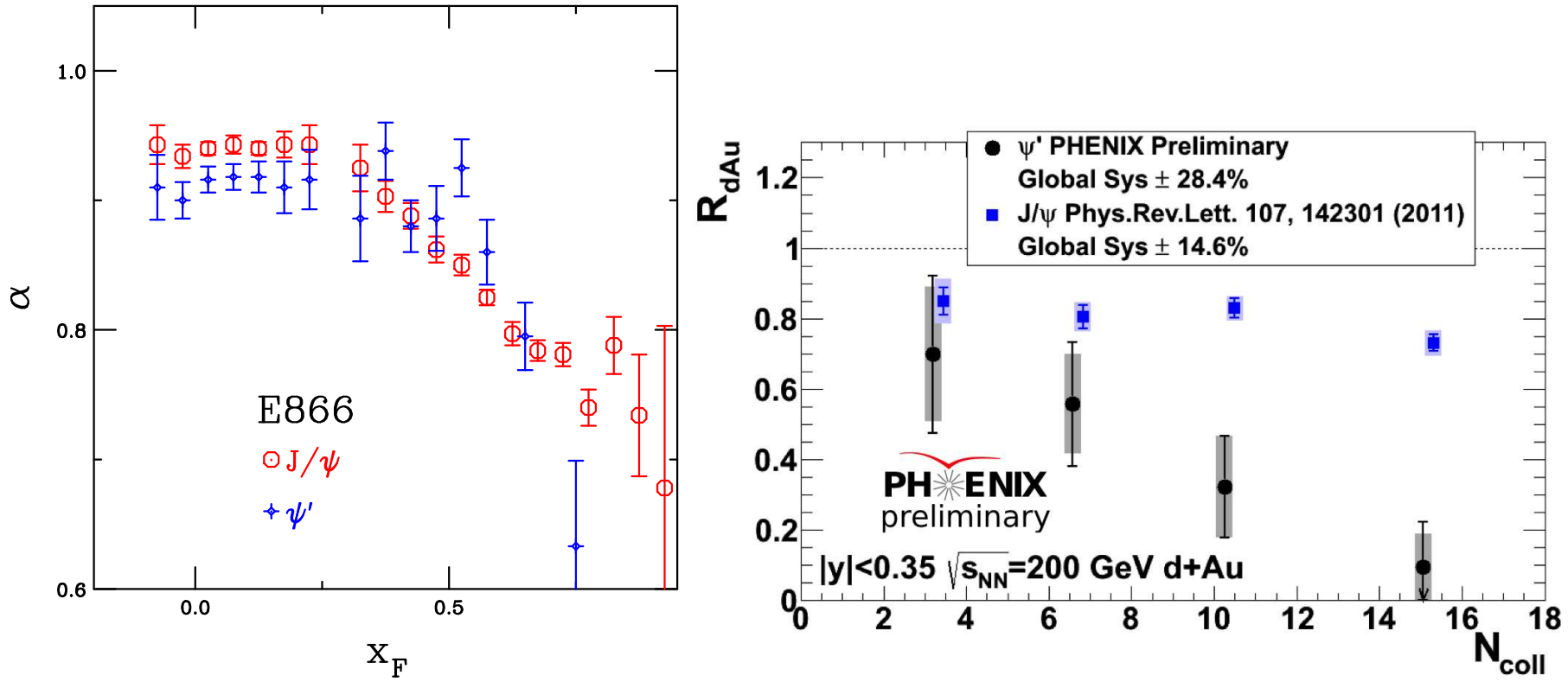


Figure 14: (Left) The $A$ dependence for $J/\psi$ and $\psi'$ production as a function of $x_F$ from E866 at FNAL ($\sqrt{s} = 38.8$ GeV). (Right) The $J/\psi$ and $\psi'$ nuclear modification as a function of collision centrality in d+Au collisions at $\sqrt{s} = 200$ GeV at RHIC.

# Effective Absorption Cross Section Energy Dependent

**Data corrected for shadowing effects here, dependence of effective absorption cross section on center of mass energy is clear, similar but weaker trend is seen even without shadowing**

**At the LHC, the absorption cross section is negligible (also, formation time stretched so that charmonium states fully formed outside the nucleus), comovers would be only possible effect**

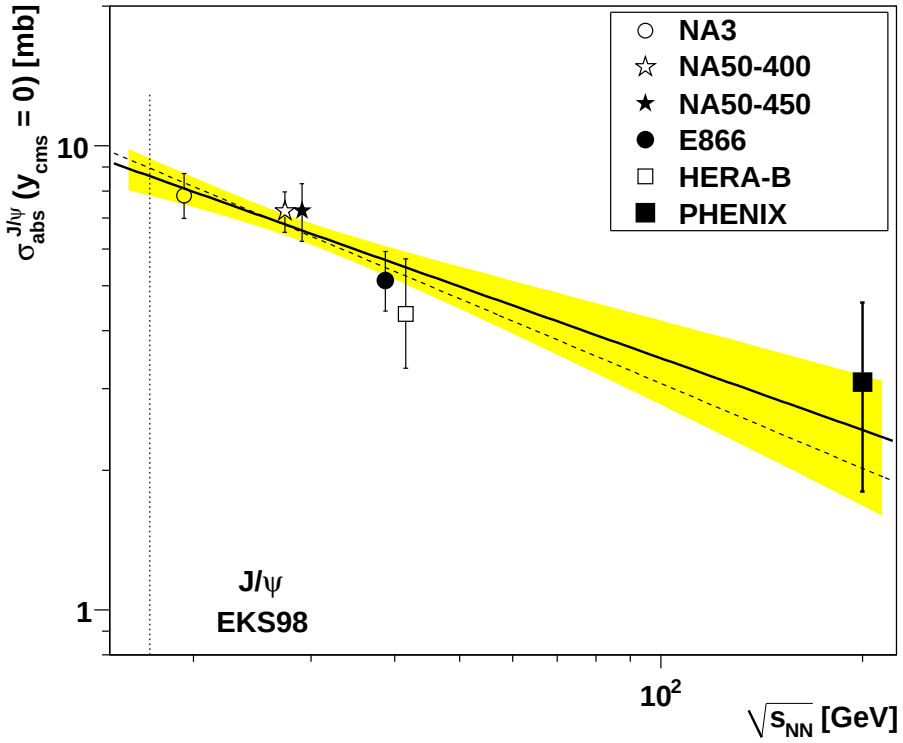


Figure 15: At midrapidity, the effective absorption cross section decreases as a function of energy. (Modified from Lourenco, Wohri and RV.)

# Intrinsic Charm

**Intrinsic charm long predicted (since 1980's) but difficult to confirm**

**Several groups have included an intrinsic component in global PDF analyses, Pumplin result from 2007 shown here, latest results from this group similar**

**IC allowed within each scenario characterized by $\langle x \rangle_{c+\bar{c}}$ at $\mu_0 = 1.3$ GeV,**

$$\langle x \rangle_{c+\bar{c}} = \int_0^1 dx\, x\, [c(x) + \bar{c}(x)]$$

**Observable consequences on the rapidity distribution at large $y$, different $A$ dependence (surface relative to volume) causes drop at large $x_F$ ($x_1$)**

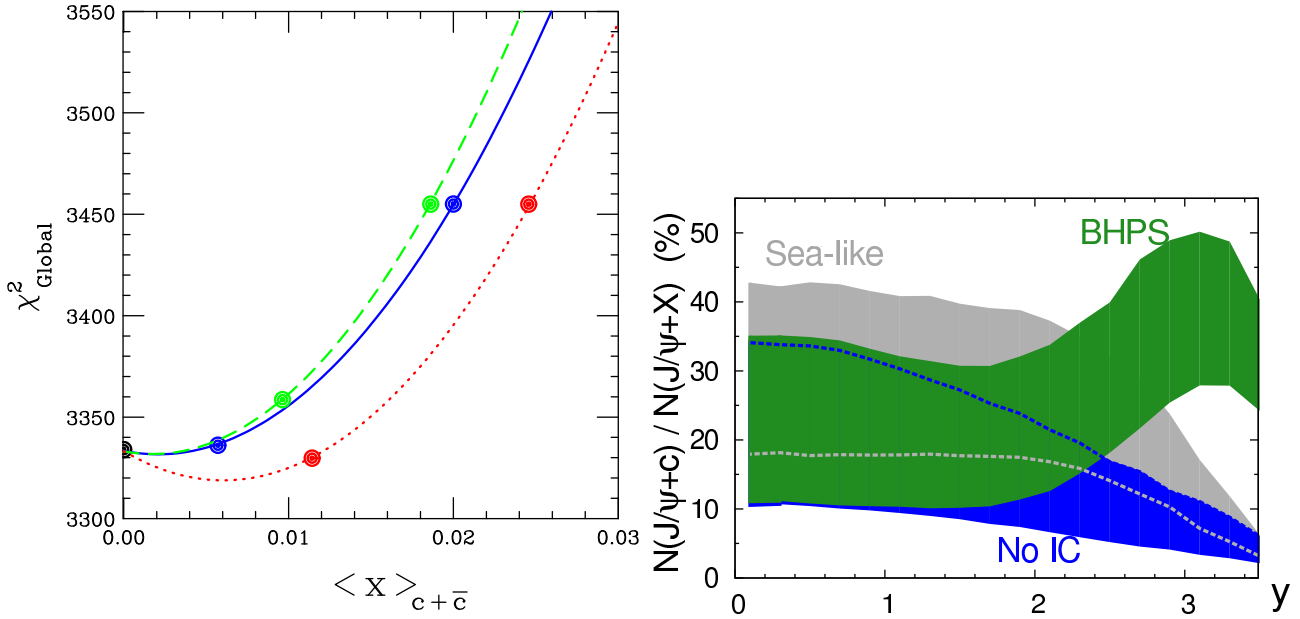


Figure 16: (Left) Goodness of fit for global analyses including IC as a function of $\langle x \rangle_{C+\bar{c}}$ for the light-cone formalism of Brodsky *et al.* (solid), the meson-cloud model (dashed); and sea-like (dotted). The lower dots correspond to candidate fits, 0.057% for Brodsky *et al.*, 0.96% for the meson cloud and 1.1% for sea-like IC. The upper dots are the most marginal fits in the different scenarios, 2% for Brodsky *et al.*, 1.9% for the meson cloud and 2.4% for sea-like. [From Pumplin *et al.*] (Right) Fraction of $J/\psi$ produced in association with a single $c$-quark ($gc \to J/\psi c$) relative to the direct yield (NLO$^+$) as a function of $y_\psi$ and for no IC, sea-like and Brodsky *et al.* (BHPS). [From Brodsky and Lansberg.]

# Shadowing Effects at the LHC

# Shadowing Parameterizations Fixed by Global Fits

Most fits (HKN, nDS, DSSZ, EKS, EPS) use available nDIS and Drell-Yan data, along with momentum sum rule and DGLAP evolution to fit a set of parameters modifying the proton PDFs

Example shown is by Eskola and collaborators

Details of fitting and data employed vary but trends are similar

Most fits now available up to NLO, FGS and EPS09s also include impact parameter dependence but other centrality parameterizations also available

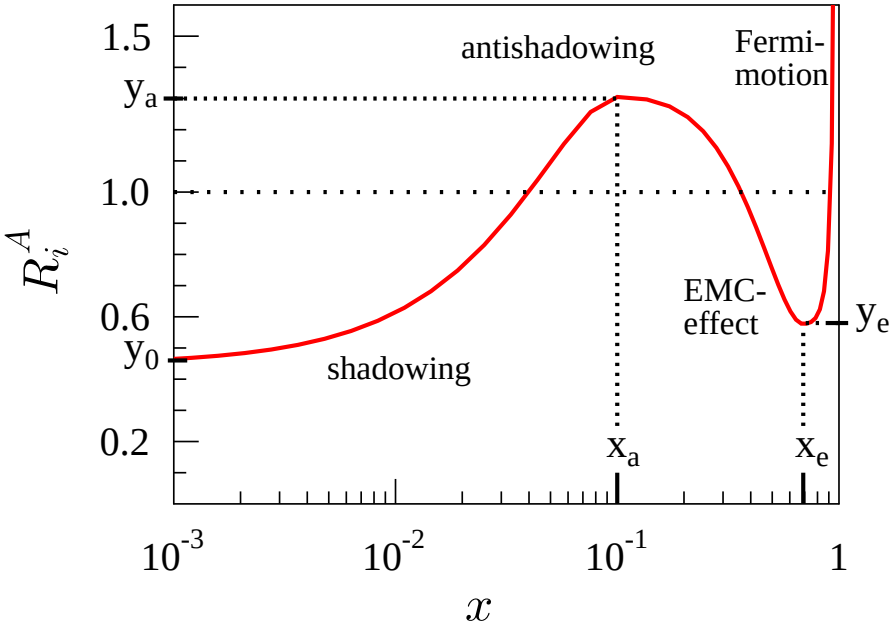


Figure 17: **An illustration of the fit function $R_i^A(x)$ for fits by Eskola *et al.*.**

# $x$ Dependence of EPS09

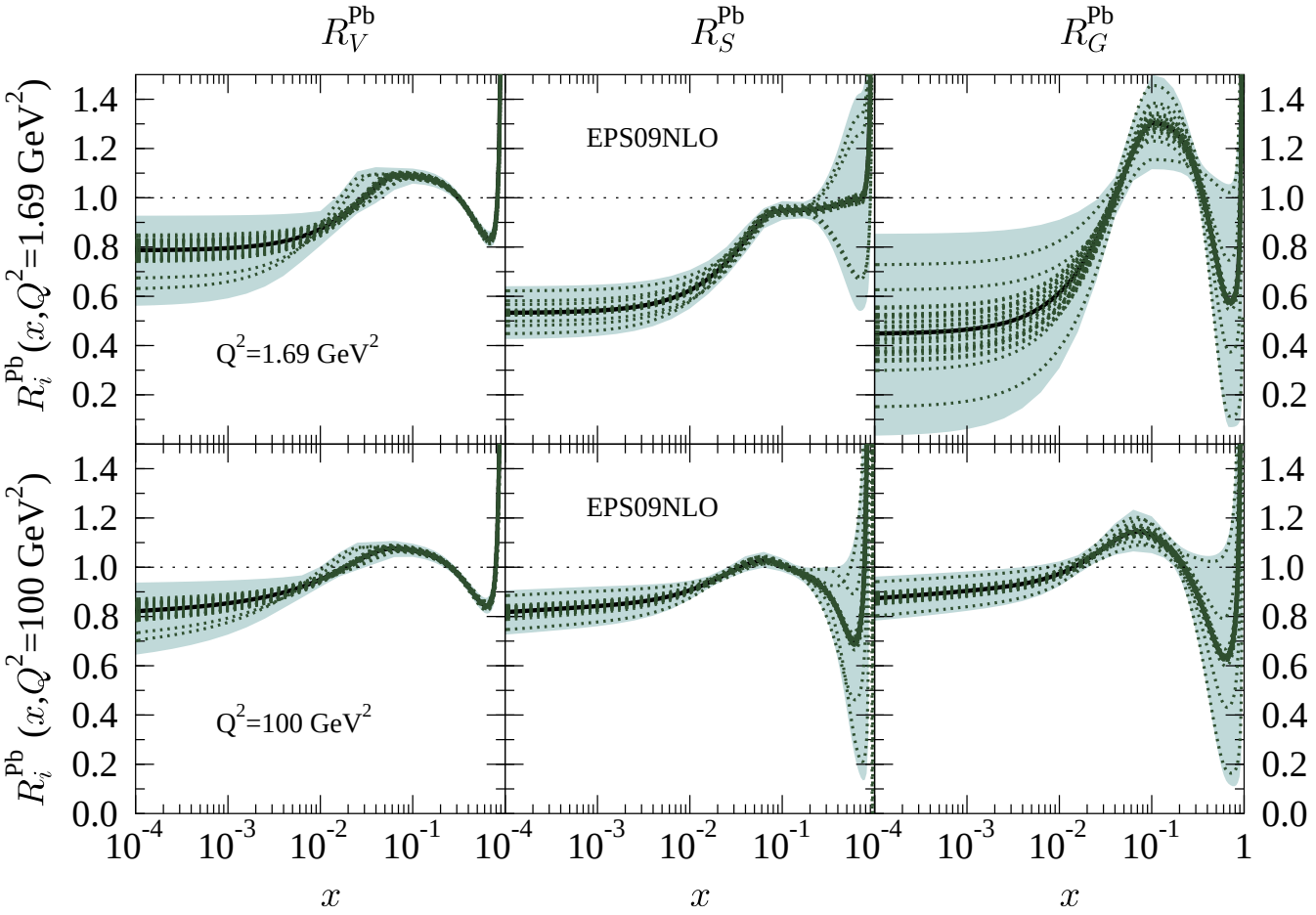


Figure 18: **The $x$ dependence of EPS09 NLO for valence (left), sea (middle) and gluon (right) distributions at $Q^2 = 1.69$ GeV$^2$ (top), the minimum value of the set, and 100 GeV$^2$ (bottom) for Pb nuclei. The darkest line in each plot is the central value, the lighter lines are the 30 error sets formed by varying each of the 15 parameters one standard deviation each side of its central value and the shaded region is the full uncertainty band.**

# $x$ Range Probed Is Very Wide at the LHC

## $x_2$ range can reach as low as $10^{-5}$ in the LHC rapidity acceptance

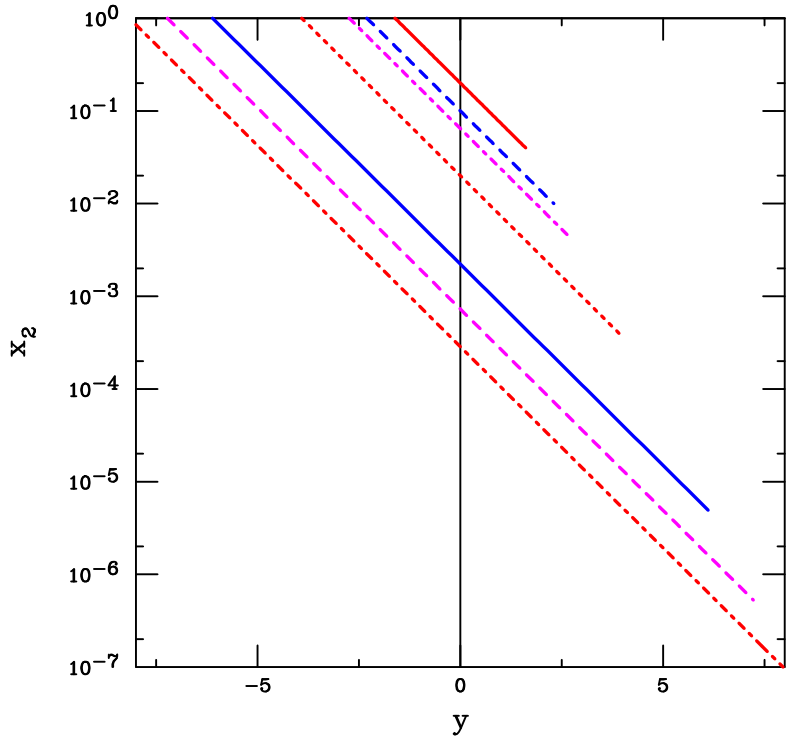


Figure 19: **(Left) The average $x_2$ as a function of rapidity for $2 \to 2$ scattering (open charm at LO, $J/\psi$ in CEM) for $\sqrt{s} = 20$, 40, 62, 200, 1800, 5500 and 14000 GeV. (Right) Gluon shadowing ratios calculated for Pb nuclei ($A = 208$) calculated at the central value of the fitted factorization scales for $J/psi$. EPS09 NLO is shown by the black solid curve while the uncertainty band is outlined by the black dotted curves. The NLO nDS and nDSg parameterizations are given in the blue dashed and blue dot dashed curves. The LO EKS98 parameterization is in magenta (dot-dot-dot-dash-dashed). The red dot-dot-dot-dashed and dot-dash-dash-dashed curves are the FGS-L and FGS-H parameterizations respectively.**

# LO and NLO Shadowing Should Agree

## LO and NLO shadowing results should agree by construction, as seen for nDS and nDSg

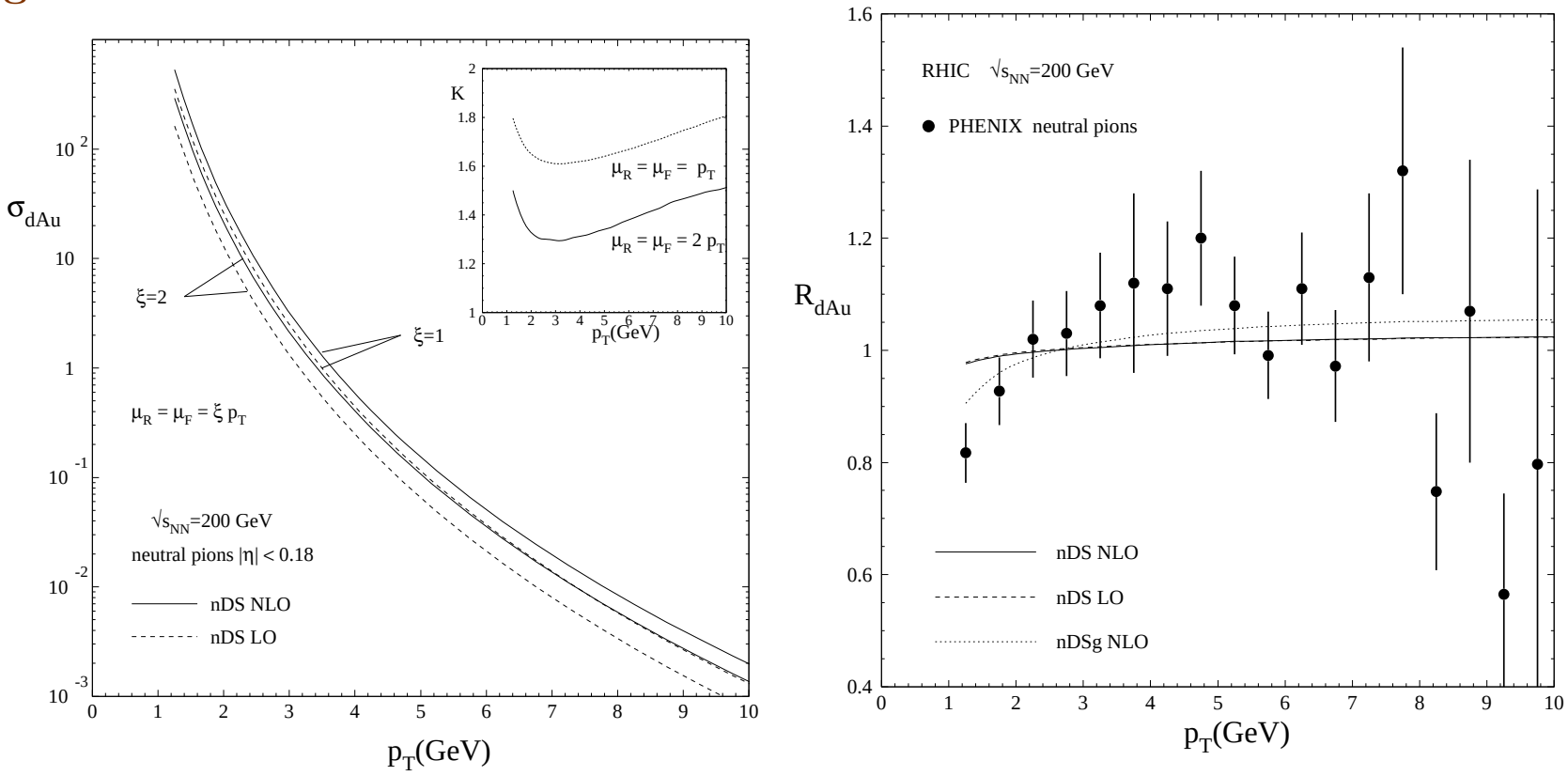


Figure 20: **(Left) The $\pi^0$ cross section in d+Au collisions at $\sqrt{s_{NN}} = 200$ GeV at LO and NLO. (Right) The LO and NLO calculations of $R_{\rm dAu}$, along with the NLO calculation with nDSg.**

# Calculating EPS09 nPDF Uncertainties in $pA$

**EPS09 LO and EPS09 NLO based on CTEQ61L and CTEQ6M respectively**

**The gluon densities in these two sets differ significantly at low $x$, hence the low $x$ modifications of EPS09 LO and NLO are quite different**

**nPDF uncertainties calculated with the 30+1 sets of EPS09: one central set and 30 sets obtained by varying each of the 15 parameters, i.e. sets 2 and 3 were obtained by changing parameter 1 by $\pm 1\sigma_1$ *etc.* where $\sigma_i$ is the standard deviation of parameter $i$**

**Uncertainties due to shadowing calculated using 30+1 error sets of EPS09 NLO added in quadrature so the uncertainty is cumulative**

# Nuclear Gluon PDFs at NLO

**EPS09 NLO and EKS98 (LO) very similar for $x > 0.002$ with significant antishadowing, nDS(g) NLO has almost none**

**nDSg and EKS98 have stronger shadowing than central EPS09 at low $x$, FGS-H(L) strongest but valid only for $x > 10^{-5}$**

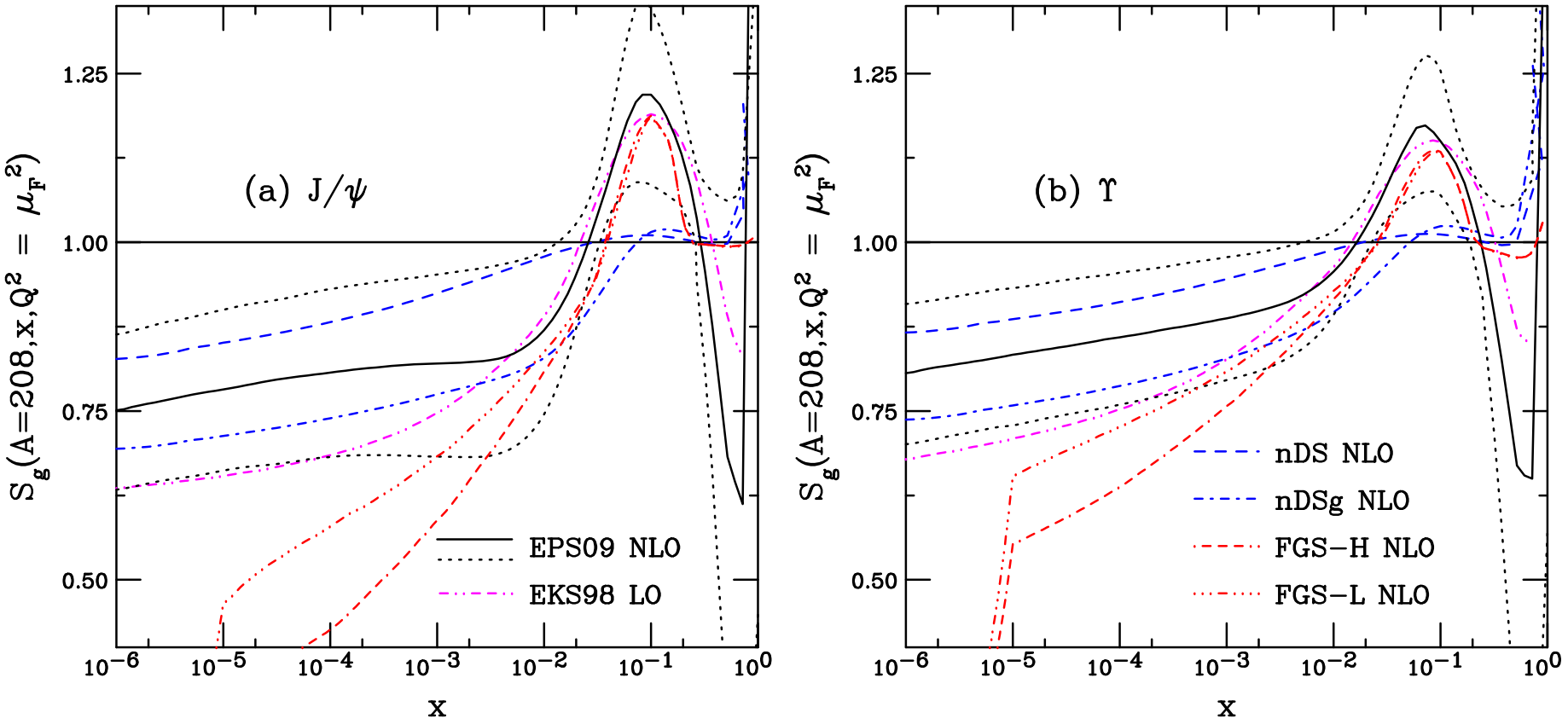


Figure 21: **Gluon shadowing ratios calculated for Pb nuclei ($A = 208$) calculated at the central value of the fitted factorization scales for $J/psi$ (a) and ϒ (b). The EPS09 NLO set is shown by the black solid curve while the uncertainty band is outlined by the black dotted curves. The NLO nDS and nDSg parameterizations are given in the blue dashed and dot-dashed curves respectively. The LO EKS98 parameterization is given in the magenta dot-dot-dash-dashed curve. The NLO FGS-H and FGS-L results are given by the red dot-dash-dash-dashed and dot-dot-dot-dashed curves respectively.**

# Suppression Factor Independent of Proton PDF

**Even though global fits (here EPS09 NLO) are based on a specific proton PDF, the calculated shadowing ratios are basically unchanged by the choice of proton PDF**

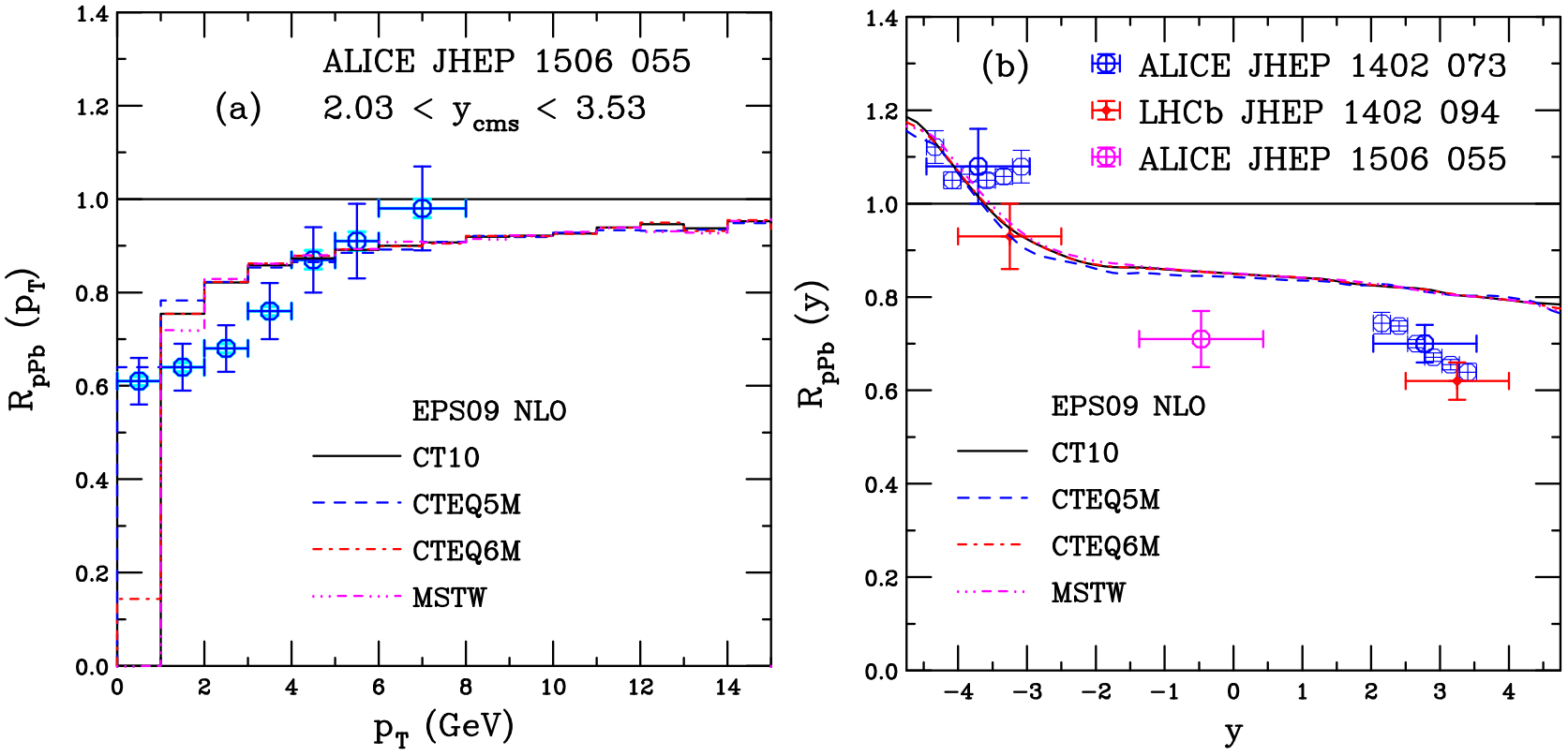


Figure 22: **The ratio $R_{p\mathrm{Pb}}(p_T)$ for ALICE at forward rapidity (left) and $p_T$-integrated as a function of rapidity. The ratios are for CT10 (black), nDS (blue), nDSg (red) and EKS98 (magenta).**

# EPS09 Uncertainty Bands I: $R_{p\mathrm{Pb}}(p_T)$

**Data typically show stronger effect than central EPS09 result alone but data tend to fall within the uncertainty band, with uncertainties for all sets added in quadrature**

**These calculations (also $R_{p\mathrm{Pb}}(y)$ and $R_{FB}$) differ somewhat from previous results shown – the wrong scale was being passed to the nPDFs**

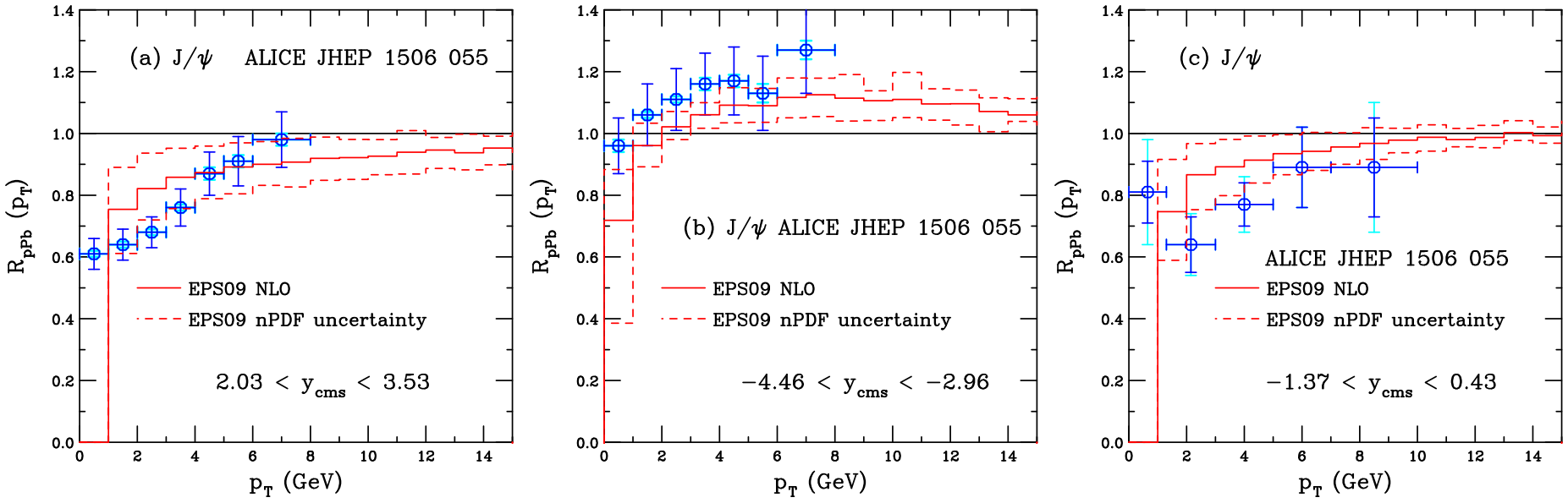


Figure 23: **The ratio $R_{p\mathrm{Pb}}(p_T)$ for ALICE at forward rapidity (left) and backward (middle) and central (right) rapidity. The EPS09 uncertainty band is shown.**

# EPS09 Uncertainty Bands II: $R_{p\mathrm{Pb}}(y)$

**Backward rapidity data agree with the rise at $y < -2.5$ from antishadowing onset**

**Preliminary midrapidity point is on the lower edge of the uncertainty band**

**Forward rapidity data are underestimated, only the lower edge of the uncertainty band (strongest shadowing) is consistent with data**

**For $y > -2.5$, the band is relatively wide, about $\pm 12\%$, and $R_{p\mathrm{Pb}}$ decreases by less than 10% in this region**

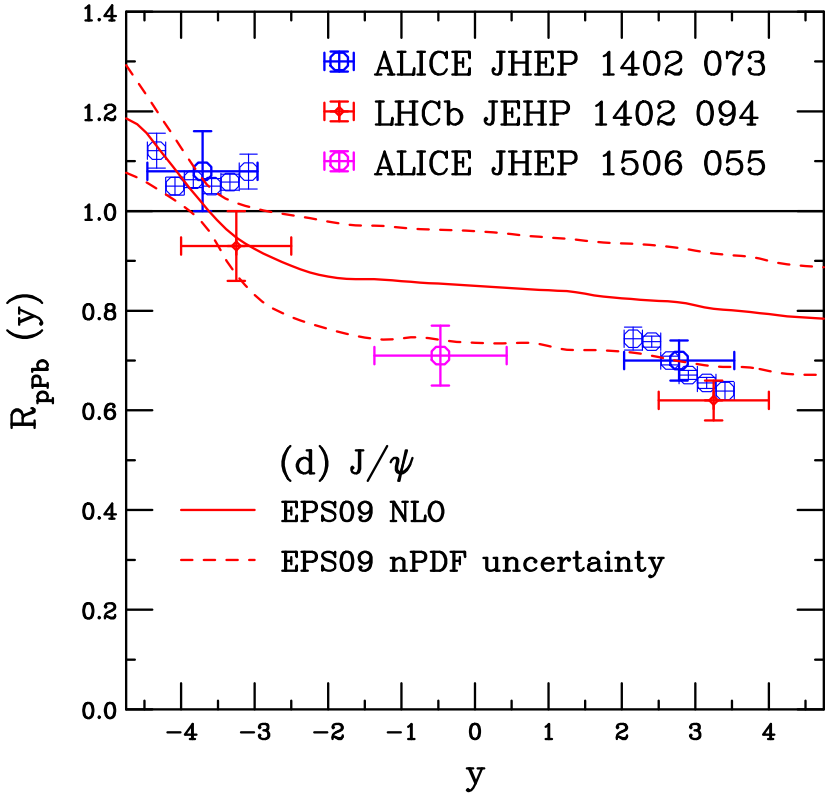


Figure 24: **The EPS09 NLO uncertainty band, $R_{p\mathrm{Pb}}(y)$.**

# EPS09 Uncertainty Bands III: $R_{FB}$

**Reduced uncertainties in the forward/backward ratio because we take the ratio before adding differences in quadrature**

**The $p_T$ ratio almost flat and above the data for $p_T < 6$ GeV**

**Curvature of rapidity ratio at $y > 2.5$ reflects the antishadowing rise at backward rapidity and the narrower uncertainty band in this region relative to the forward region**

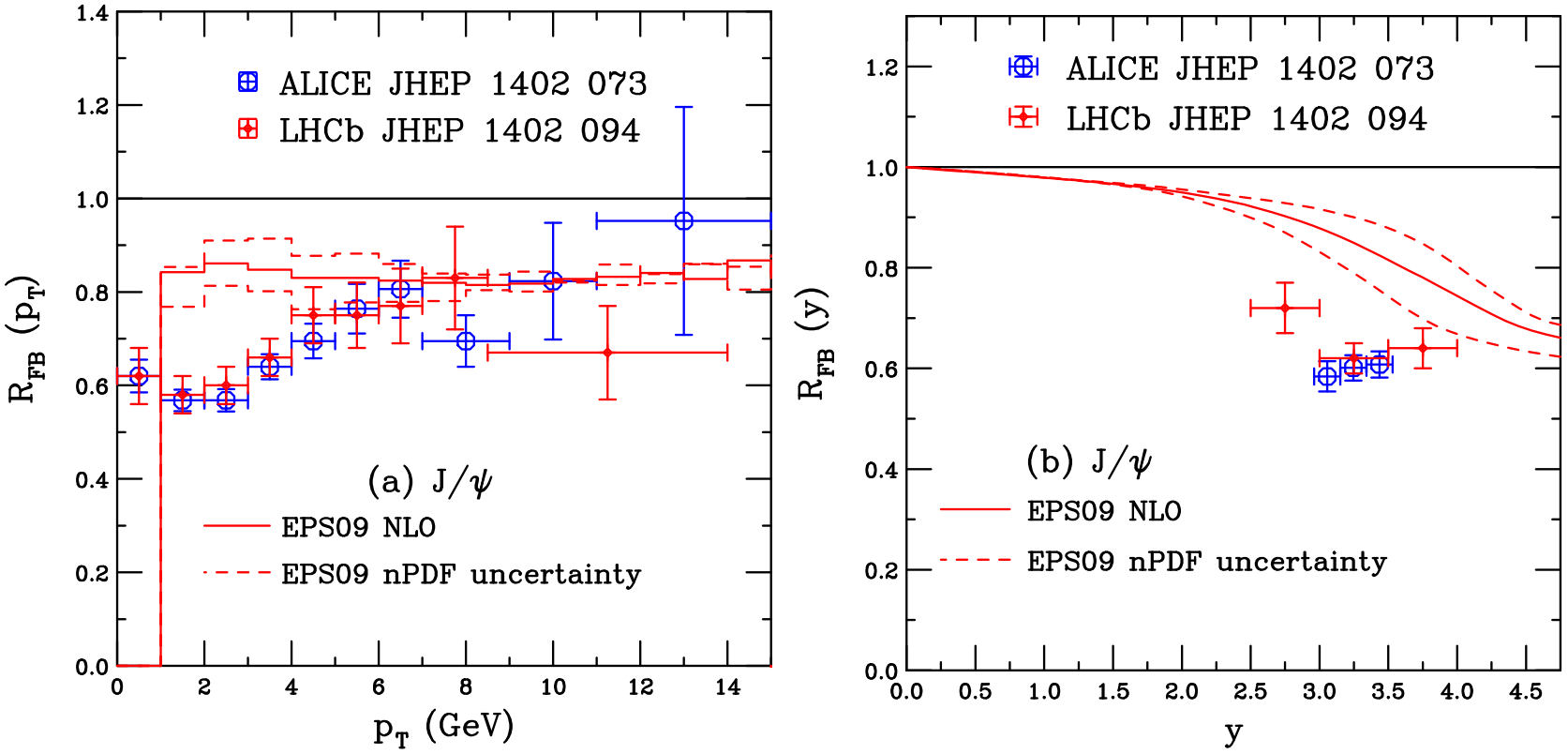


Figure 25: **The ratio $R_{p\mathrm{Pb}}(p_T)$ for ALICE at forward rapidity (left) and $p_T$-integrated as a function of rapidity (right). The EPS09 uncertainty band is shown.**

# NLO vs LO EPS09

**The nPDF set should be appropriate to the order of the calculation: if using the LO set in a NLO calculation agrees better with the data, it isn't really better**

**NLO calculation required for CEM $p_T$ distribution and is more appropriate**

**LO CEM uncertainty band is broader, with stronger shadowing, to counterbalance the flatter low $x$ behavior of CTEQ61L while CTEQ6M is valence-like: different behavior of proton PDFs makes good order-by-order agreement of $R_{p\mathrm{Pb}}$ difficult**

**Starting scale of EPS09 is 1.69 GeV$^2$, same as CTEQ6 starting scale**

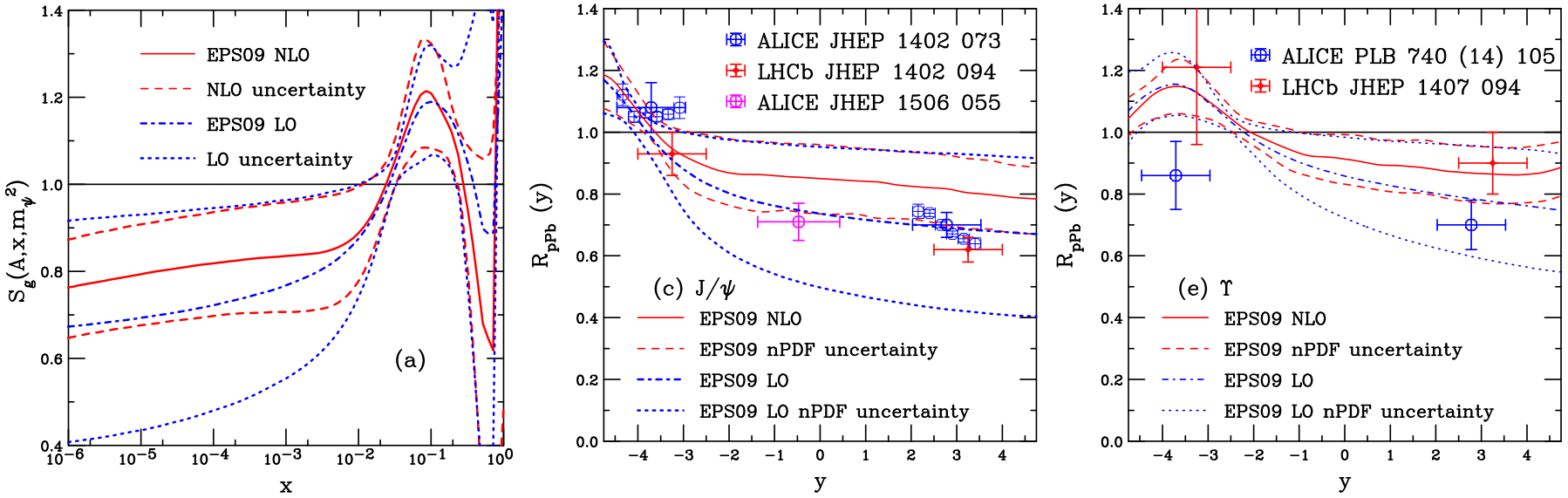


Figure 26: **(Left) The EPS09 LO (blue) and NLO (red) uncertainty bands for gluon shadowing. The corresponding uncertainty bands for $R_{p\mathrm{Pb}}(y)$ at $\sqrt{s_{NN}} = 5$ TeV for $J/\psi$ (center) and $\Upsilon$ (right).**

# NLO vs LO nDS

**While there are some differences between the LO and NLO nDS and nDSg ratios, especially for nDSg at $x \sim 0.01$, the LO and NLO ratios are much closer than those of the EPS09 central sets, here order of calculation is not an issue**

**nDS(g) employs GRV98 LO and NLO proton PDFs, the $Q^2$ range of the nPDF, $1 < Q^2 < 10^6$ GeV$^2$, is above the minimum scale of GRV98, unlike EPS09 and CTEQ6**

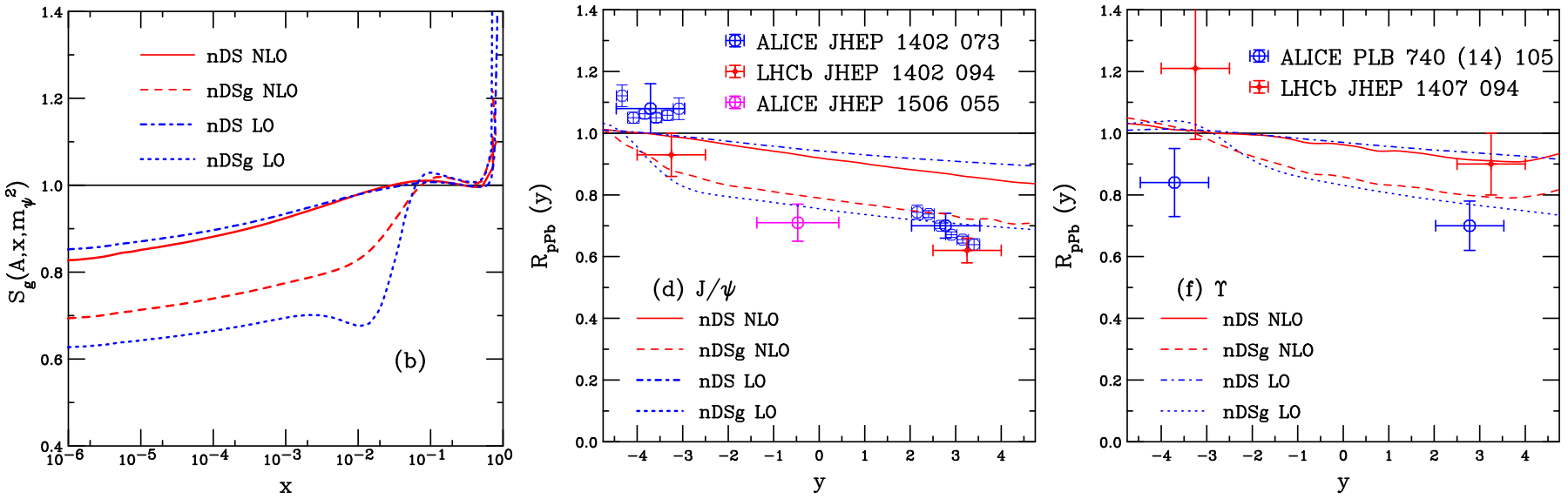


Figure 27: **(Left) The nDS and nDSg LO (blue) and NLO (red) gluon shadowing ratios. The corresponding results for $R_{p\mathrm{Pb}}(y)$ at $\sqrt{s_{NN}} = 5$ TeV are shown for $J/\psi$ (center) and $\Upsilon$ (right).**

# EPS09 vs Other nPDFs I: $R_{p\mathrm{Pb}}(p_T)$

**Central EPS09 NLO set compared to nDS NLO, nDSg NLO and EKS98 (LO)**

**nDS effect is weakest of all while nDSg is weak at backward rapidity but stronger than EPS09 at mid- and forward rapidity**

**EKS98 and EPS09 NLO are very similar for $x > 0.01$ so they agree well at backward and mid-rapidity while EKS98 is stronger at forward rapidity**

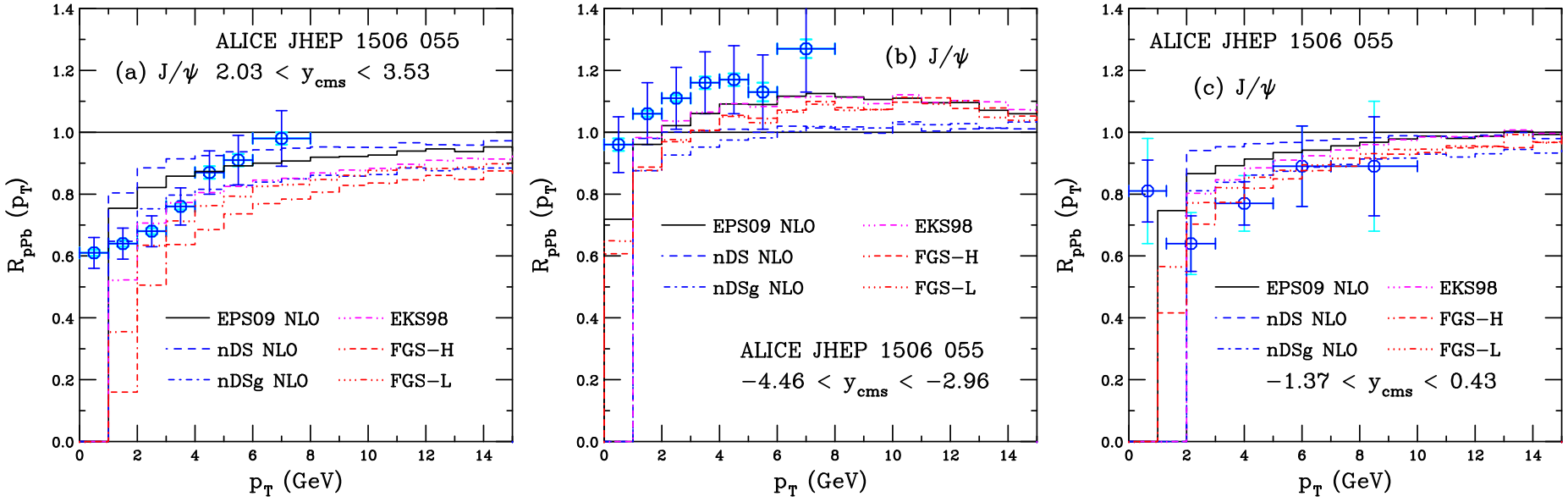


Figure 28: **The ratio $R_{p\mathrm{Pb}}(p_T)$ for ALICE at forward (left), backward (center) and mid- (right) rapidity. The ratios are for central EPS09 NLO (black), nDS NLO (blue), nDSg NLO (red) and EKS98 LO (magenta).**

# EPS09 vs Other nPDFs II: $R_{p\mathrm{Pb}}(y)$

**EKS98 LO follows EPS09 NLO central set until $y > -2$ where it decreases linearly while EPS09 becomes flatter**

**EPS09 abrupt change of slope near antishadowing region follows from the gluon shadowing ratio, almost like the low $x$ behavior had to join to assumed antishadowing shape at intermediate $x$**

**nDS and nDSg, with no antishadowing, have a weaker $y$ dependence overall**

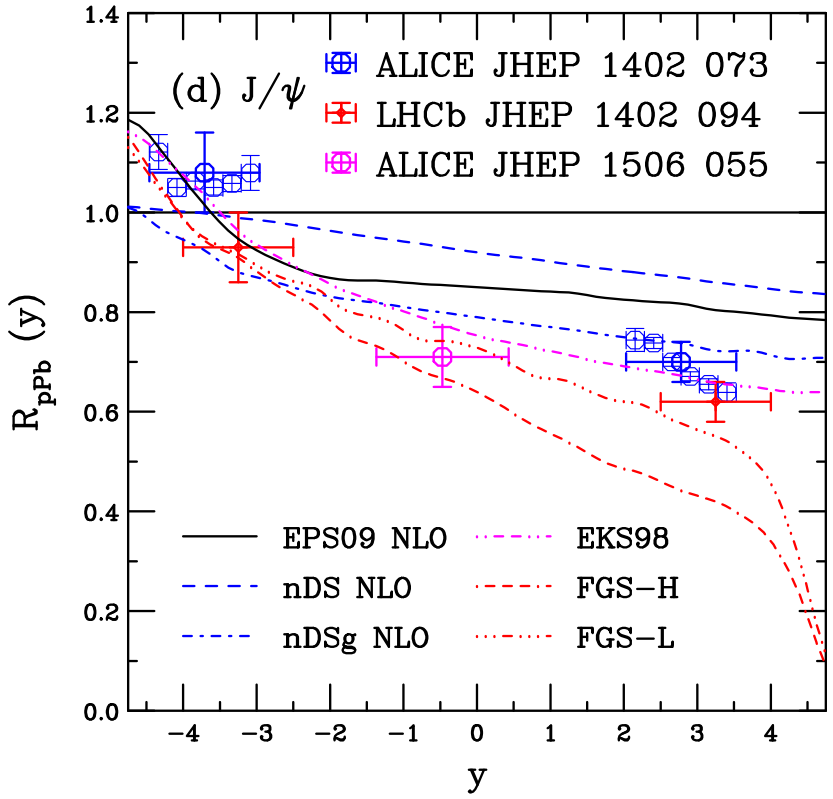


Figure 29: **The calculated $R_{p\mathrm{Pb}}(y)$ for central EPS09 NLO (black), nDS NLO (blue), nDSg NLO (red) and EKS98 LO (magenta).**

# EPS09 vs Other nPDFs III: $R_{FB}$

**nDS has strongest $p_T$ dependence of $R_{FB}(p_T)$, EKS98 comes closest to agreement with low $p_T$ data due to the stronger effect at low $x$ than EPS09**

**Only EPS09 shows curvature in $R_{FB}(y)$, the others show an almost linear $y$ dependence**

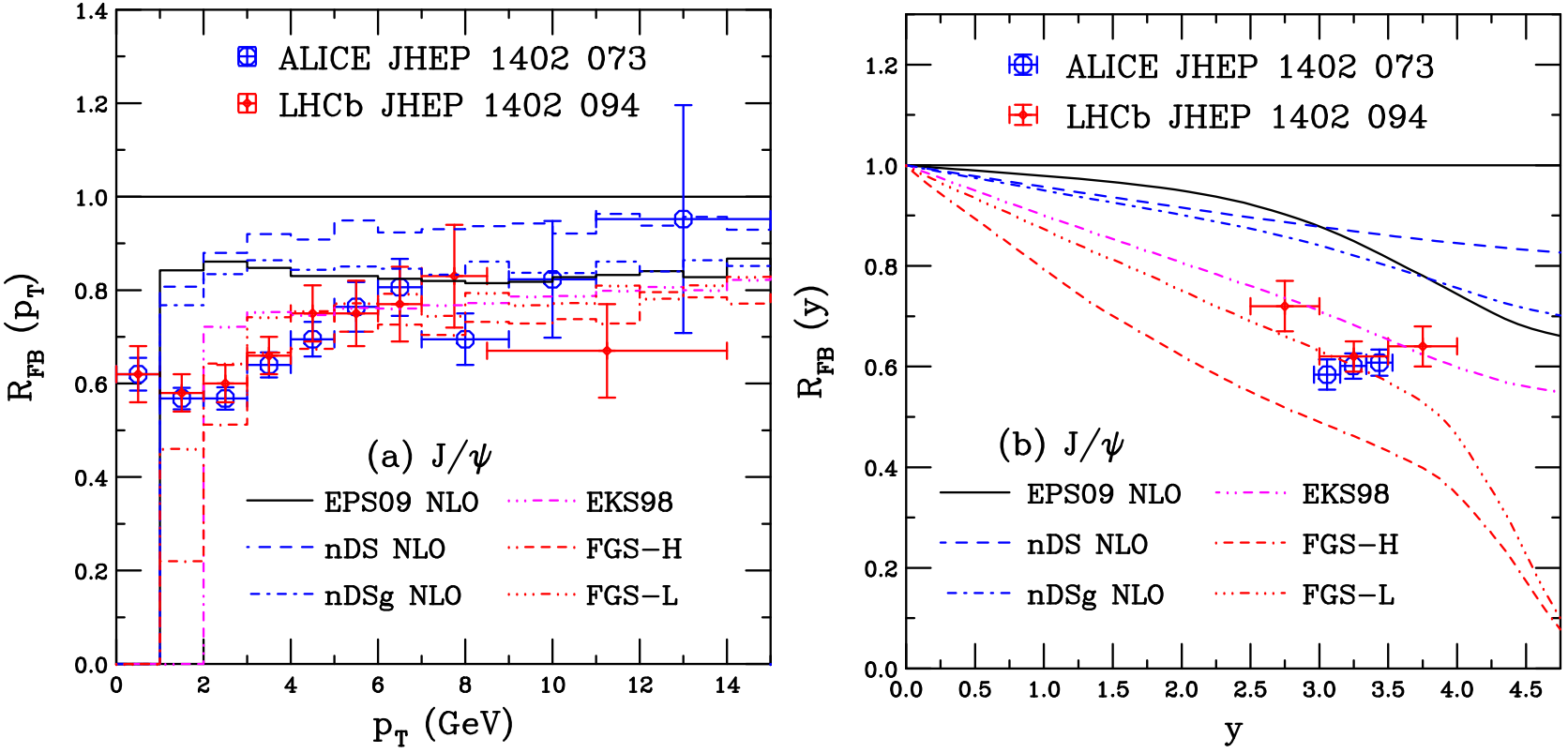


Figure 30: **The ratio $R_{p\mathrm{Pb}}(p_T)$ for ALICE at forward rapidity (left) and $p_T$-integrated as a function of rapidity. The ratios are for central EPS09 NLO (black), nDS NLO (blue), nDSg NLO (red) and EKS98 LO (magenta).**

# EPS09 vs Other nPDFs IV: $\Upsilon$ $R_{p\mathrm{Pb}}(y)$, $R_{FB}(y)$

**Generally relatively good agreement with $R_{p\mathrm{Pb}}$**

**Rather narrow antishadowing band for FGS sets**

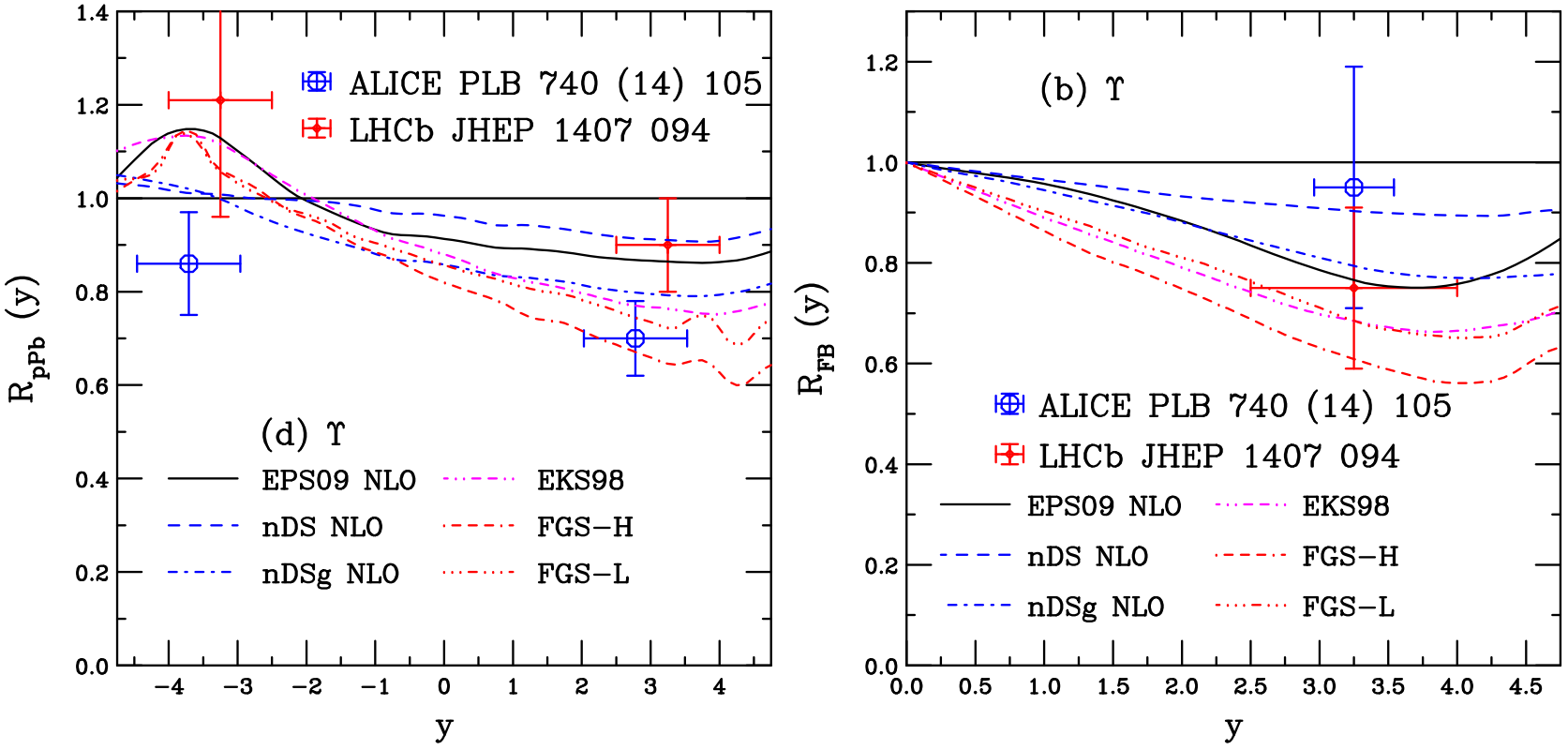


Figure 31: **The ratio $R_{p\mathrm{Pb}}(y)$ for ALICE at forward rapidity (left) and $p_T$-integrated as a function of rapidity. The ratios are for central EPS09 NLO (black), nDS NLO (blue dashed), nDSg NLO (blue dot dashed), EKS98 LO (magenta), FGS-H NLO (red dot-dash-dash-dashed) and FGS-L NLO (red dot-dot-dot-dashed).**

# Calculating Mass and Scale Uncertainties

**We calculate the mass and scale uncertainties in 3 ways:**

**The first two follow Cacciari, Nason and RV where the cross section extremes with mass and scale are used to calculate the uncertainty**

$$\sigma_{\rm max} = \sigma_{\rm cent} + \sqrt{(\sigma_{\mu,\rm max} - \sigma_{\rm cent})^2 + (\sigma_{m,\rm max} - \sigma_{\rm cent})^2} \ ,$$
$$\sigma_{\rm min} = \sigma_{\rm cent} - \sqrt{(\sigma_{\mu,\rm min} - \sigma_{\rm cent})^2 + (\sigma_{m,\rm min} - \sigma_{\rm cent})^2} \ ,$$

$m/\mu_F/\mu_R$ **v1 We initially take the ratios of $p$+Pb to $pp$ for each mass and scale combination and then locate the extrema in each case – this gives the uncertainty on $R_{p\rm Pb}$ of each set, can appear odd if ratios are not very different but the extrema changes between sets**

$m/\mu_F/\mu_R$ **v2 We locate the mass and scale extrema and calculate the uncertainty as above and then form $R_{p\rm Pb}$ by dividing by the $pp$ cross section calculated with the central parameter set – this forms global $R_{p\rm Pb}$ based on the cross sections rather than the shadowing ratios and is thus significantly larger, especially at low $p_T$, becoming smaller at high $p_T$ (Does not apply to $R_{FB}$)**

$m/\mu_F/\mu_R$ **v3 We add the mass and scale uncertainties in quadrature, a la EPS09, and then form $R_{p\rm Pb}$ by dividing by the central $pp$ cross section – since this is a cumulative uncertainty rather than based on the greatest excursion from the mean, it is the largest uncertainty at low $p_T$. This was calculated assuming that the appropriate $\mu_F/m$ and $\mu_R/m$ pairs are $[(H,H),(L,L)]$, $[(H,C),(L,C)]$ and $[(C,H),(C,L)]$, other choices could lead to different results**

# Mass and Scale Uncertainty Bands I: $R_{p\mathrm{Pb}}(p_T)$

**Uncertainties based on the differences due to EPS09 NLO alone, *i.e.* taking the extrema based on the ratios, gives very small uncertainty, smaller than EPS09 NLO**

**Uncertainties based on cross sections are much larger with v3 bigger than v2 at low $p_T$, expected since ratio is cumulative**

**Ratios decrease at high $p_T$ where the scale choices are less important since $p_T \gg m$**

**$\Upsilon$ uncertainties narrower than $J/\psi$**

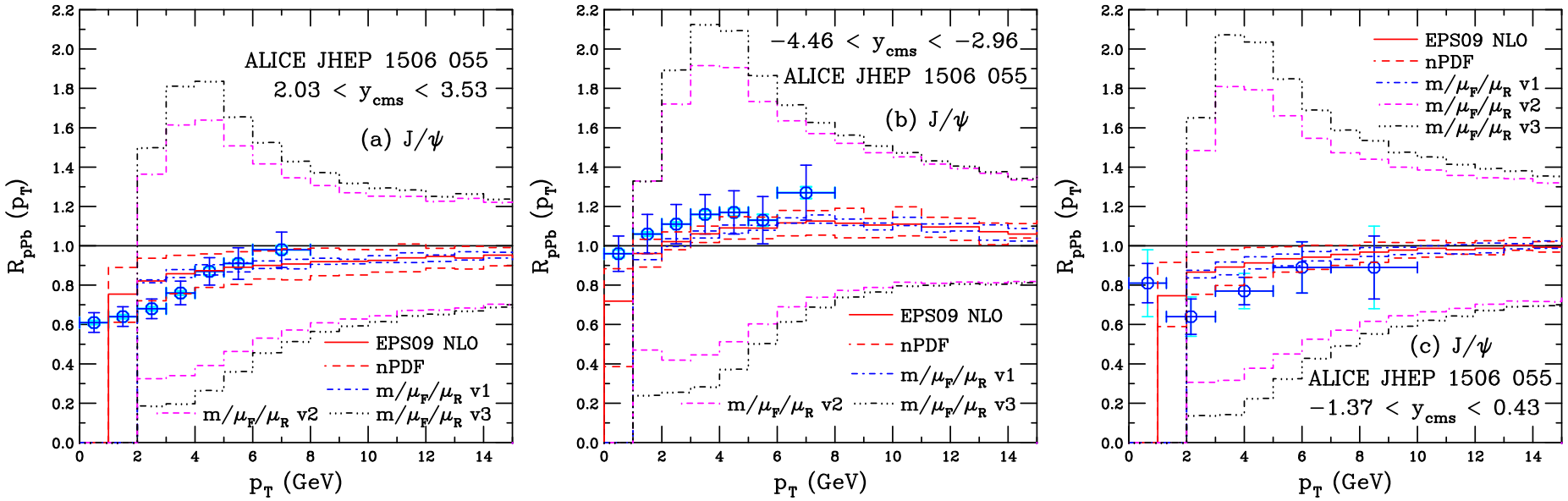


Figure 32: **The mass and scale uncertainties in the ratio $R_{p\mathrm{Pb}}(p_T)$ are compared to those for EPS09 NLO alone for ALICE at forward (left), backward (middle) and mid- (right) rapidity. The EPS09 uncertainty band is shown in red while the uncertainties calculated with method v1 in blue, v2 in magenta and v3 in black.**

# Mass and Scale Uncertainty Bands II: $R_{p\mathrm{Pb}}(y)$

**Rapidity dependence with v1 exhibits the perils(?) of basing extrema on individual $R_{p\mathrm{Pb}}$ ratios – when one ratio is larger at high $|y|$ but not at midrapidity, the calculated v1 changes slope at the switching point**

**Right-hand plot indicates how this happens, the ratio with $(H, H)$ is larger than that of the next highest ratio, that with $(C, L)$ except for $|y| < 2$**

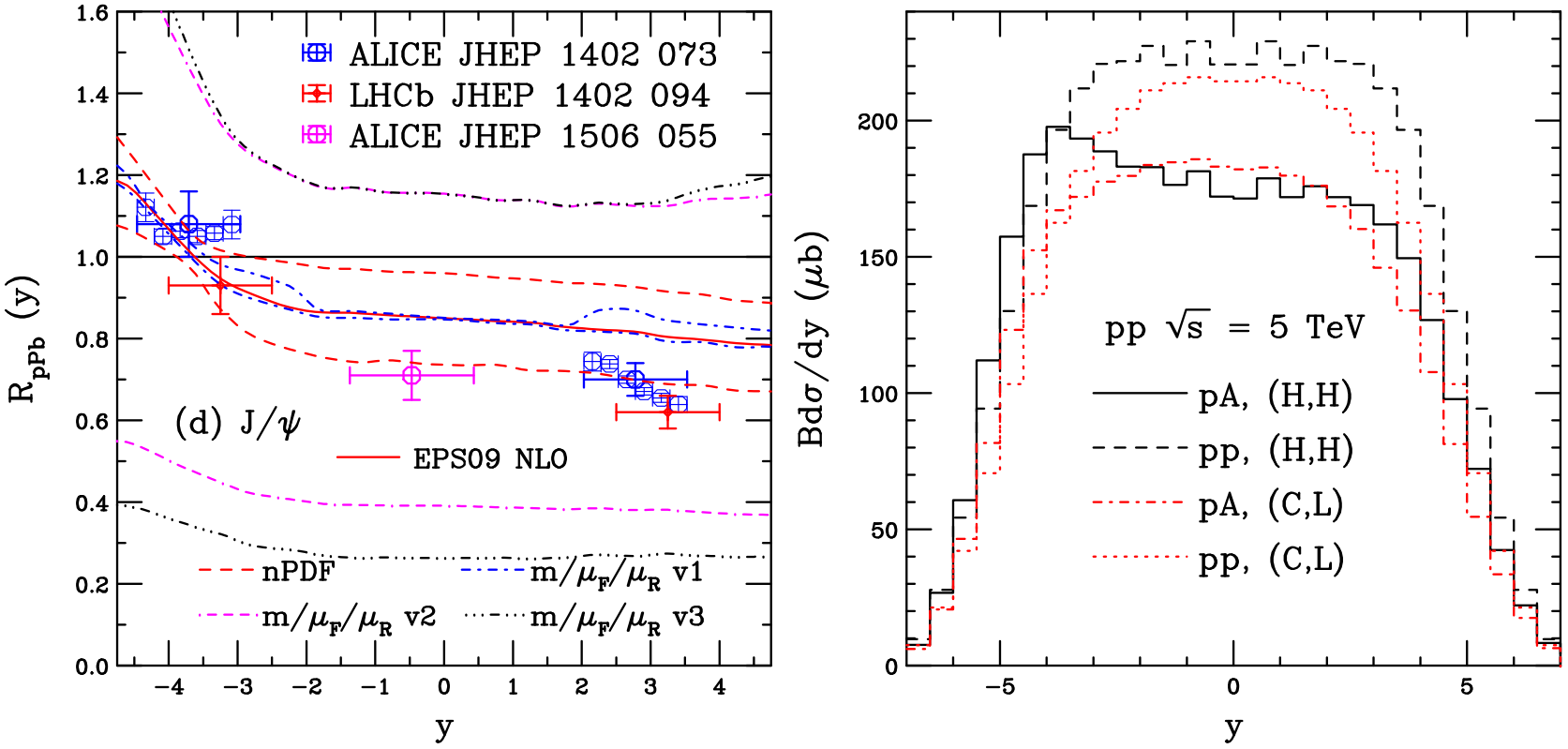


Figure 33: **(Left) The mass and scale uncertainties in the ratio $R_{p\mathrm{Pb}}(y)$ are compared to those for EPS09 NLO alone. The EPS09 uncertainty band is shown in red while the uncertainties calculated with method v1 in blue, v2 in magenta and v3 in black. (Right) The $pp$ and $p$+Pb rapidity distributions for the $(H, H)$ $(C, L)$ sets showing the differences leading to the change in the upper limit of the mass and scale uncertainties of method v1 around midrapidity.**

# Mass and Scale Uncertainty Bands III: $R_{FB}$

**Only v1 and v3 apply here (v2 is equivalent to v1 in this case)**

**Taking the forward to backward ratio before calculating the uncertainty band makes this ratio essentially insensitive to the mass and scale**

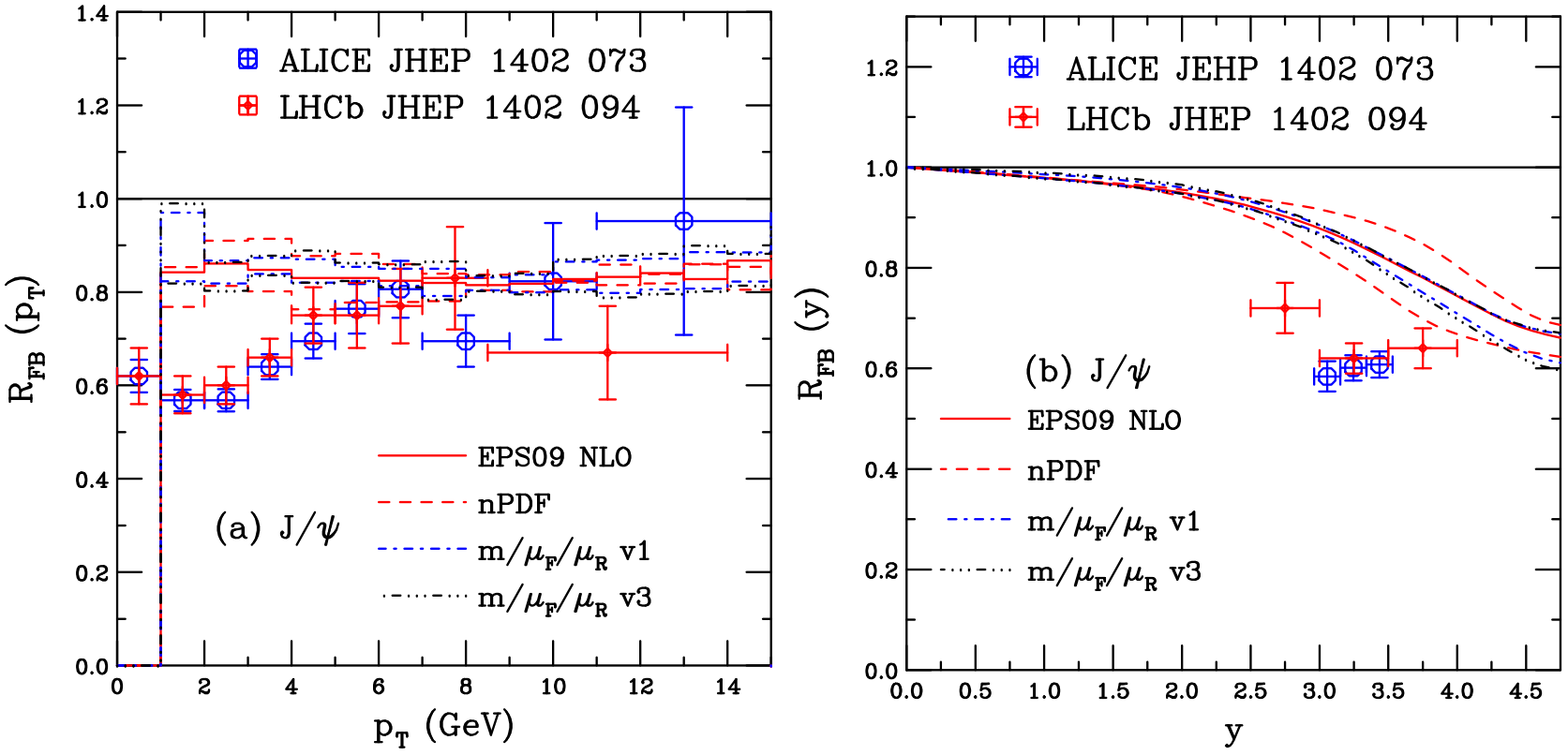


Figure 34: **The mass and scale uncertainties in the ratios $R_{FB}(p_T)$ (left) and $R_{FB}(y)$ (right) are compared to those for EPS09 NLO alone for ALICE at forward (left), backward (middle) and mid- (right) rapidity. The EPS09 uncertainty band is shown in red while the uncertainties calculated with method v1 in blue, v2 in magenta and v3 in black.**

# Mass and Scale Uncertainty Bands IV: $\Upsilon$ $R_{p\mathrm{Pb}}(y)$, $R_{FB}(y)$

## Mass and scale uncertainty narrower on $R_{p\mathrm{Pb}}$ for $\Upsilon$ than for $J/\psi$

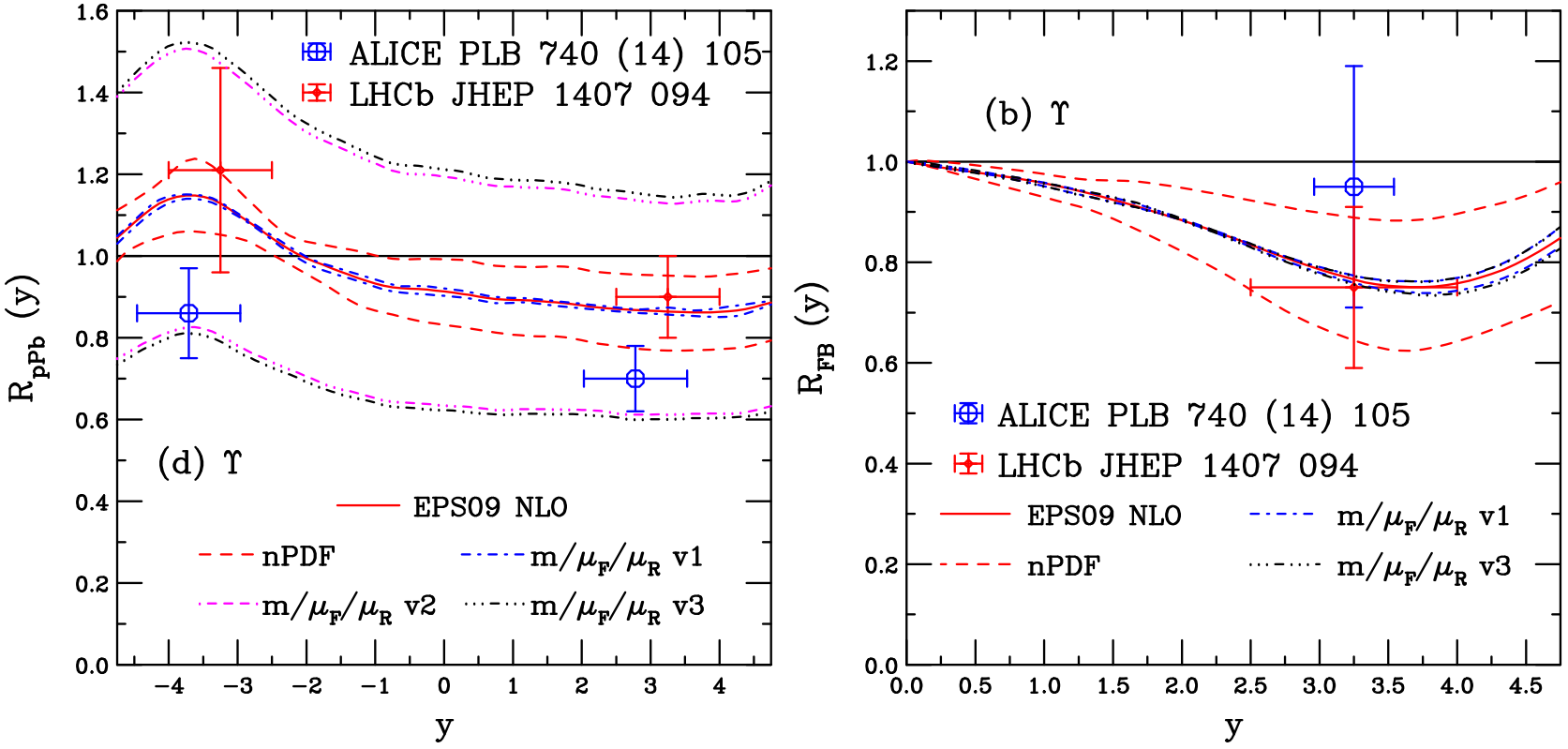


Figure 35: **The mass and scale uncertainties in the ratios $R_{p\mathrm{Pb}}(y)$ (left) and $R_{FB}(y)$ (right) are compared to those for EPS09 NLO alone for ALICE at forward (left), backward (middle) and mid- (right) rapidity. The EPS09 uncertainty band is shown in red while the uncertainties calculated with method v1 in blue, v2 in magenta and v3 in black.**

# Factorization of $R_{AA}$ into $R_{pA}(+y) \times R_{pA}(-y)$? $J/\psi$

**The factorization is exact for the CEM at LO because the process is $2 \to 1$ and the scale is fixed ($p_T = 0$) so $x_1$ and $x_2$ are known at each $y$ – compare red line with circles on the left**

**Factorization is not automatic at NLO because process is $2 \to 2\,[(c\overline{c}) + g/q/\overline{q}]$ and the additional parton makes the correspondence between $x_1, x_2$ and $y$ inexact, even at fixed rapidity – agreement is good, nevertheless**

**Works well for $\Upsilon$ also**

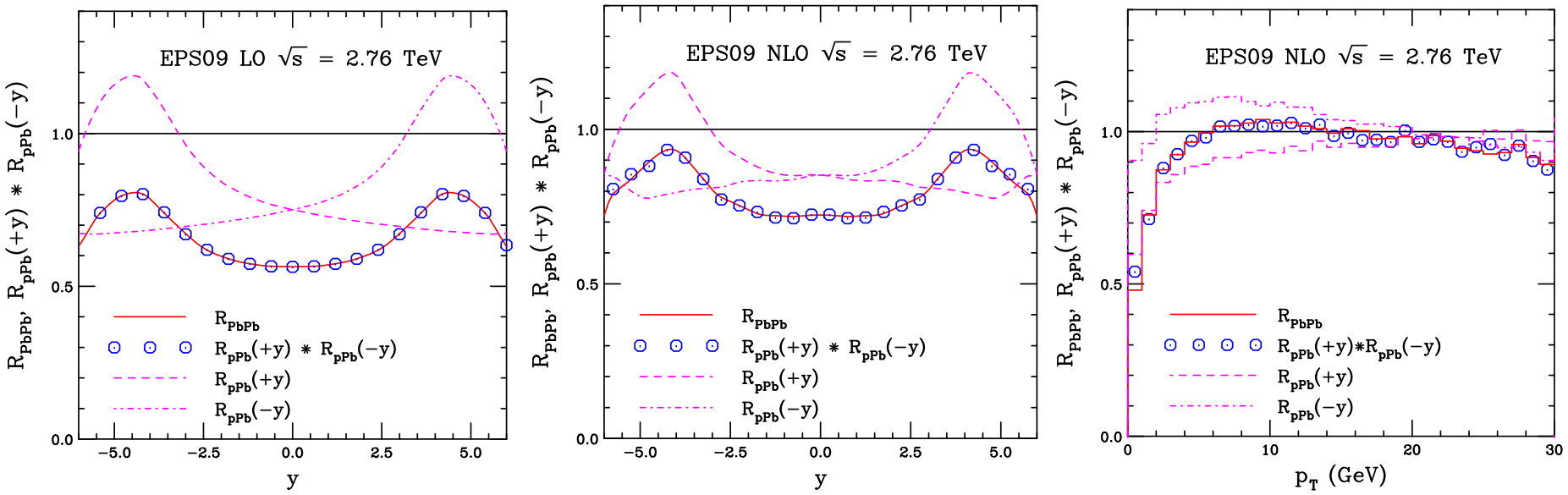


Figure 36: **The $R_{AA}$ (red) ratio is compared to the product $R_{pA}(+y) \times R_{pA}(-y)$ (points) along with the individual $pA$ ratios at forward (dashed) and backward (dot-dashed) rapidity. Results are compared for the rapidity distributions at LO (left) and NLO (middle) as well as for the $p_T$ dependence at NLO (right).**

# Factorization of $R_{AA}$ into $R_{pA}(+y) \times R_{pA}(-y)$? $\Upsilon$

**Agreement also good for $\Upsilon$ production even though there is somewhat more scatter at high $p_T$**

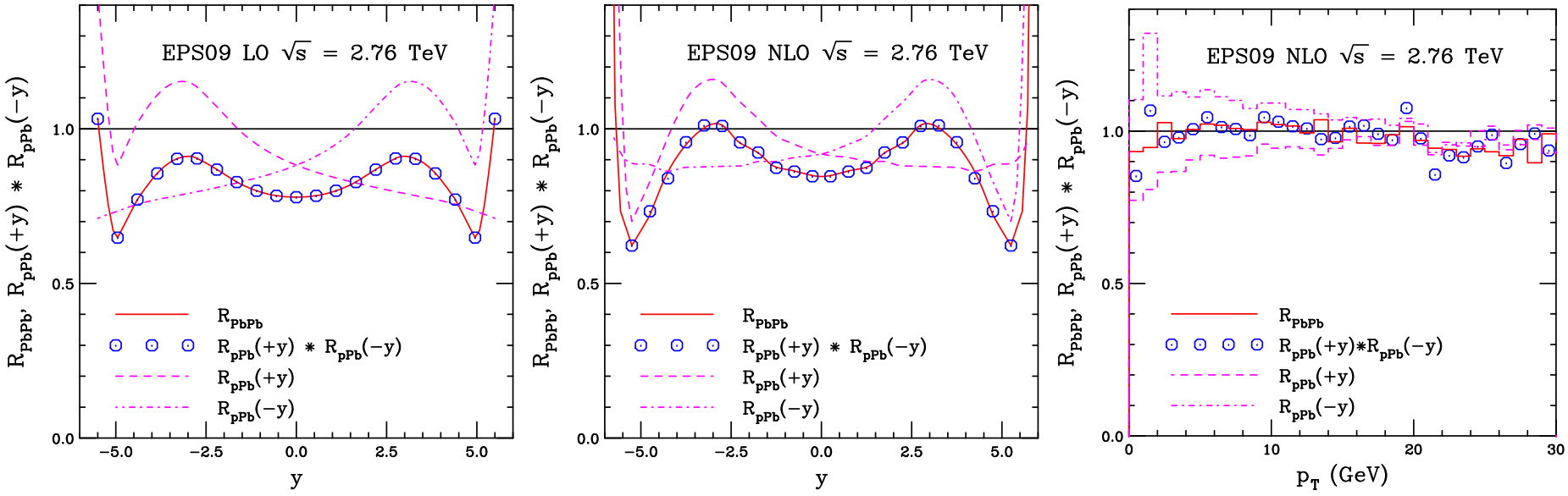


Figure 37: **The $R_{AA}$ (red) ratio is compared to the product $R_{pA}(+y) \times R_{pA}(-y)$ (points) along with the individual $pA$ ratios at forward (dashed) and backward (dot-dashed) rapidity. Results are compared for the rapidity distributions at LO (left) and NLO (middle) as well as for the $p_T$ dependence at NLO (right).**

# Summary

- Fitting the scale parameters to the total $Q\overline{Q}$ cross section data significantly reduces the uncertainties on open heavy flavor and quarkonium production
- Differences in LO and NLO results for EPS09 on $J/\psi$ production illustrates the fact that gluon nPDF is still not very well constrained, although, given the approximate concordance of the nDS results, the EPS09 discrepancy may be due to the choice of CTEQ6 proton PDFs
- LHC $p$+Pb hadroproduction data could be taken into global analyses in the future but many caveats on medium effects, *e.g.* initial and/or final state energy loss, production mechanism, saturation effects – while the $R_{p\mathrm{Pb}}$ results, both as a function of $p_T$ and $y$, look good, the $R_{FB}$ results are not as good: $pp$ data at 5 TeV are required
- Excited states more subject to comovers (not discussed here) because they are larger